NTNU – Trondheim
Norwegian University of
Science and Technology

Intragranular Chromium Nitride Precipitates in Duplex and Superduplex Stainless Steel

Torunn Hjulstad Iversen

Materials Science and Engineering
Submission date: June 2012
Supervisor: Jan Ketil Solberg, IMTE
Co-supervisor: Mads Aursand, Statoil

Norwegian University of Science and Technology
Department of Materials Science and Engineering

Abstract

Intragranular chromium nitrides is a phenomenon with detrimental effects on material properties in superduplex stainless steels which have not received much attention. Precipitation of nitrides occurs when the ferritic phase becomes supersaturated with nitrogen and there is insufficient time during cooling for diffusion of nitrogen into austenite. Heat treatment was carried out at between 1060°C and 1160°C to study the materials susceptibility to nitride precipitation with varying heat treatment temperature, nitrogen content and microstructure. Microhardness tests and Charpy v-notch tests were also carried out to investigate the nitrides effect on material properties. No standard method of quantification of nitrides exist. A method of quantifying the precipitation based on area fraction of nitrides was therefore introduced. The results show an increased amount of nitride precipitation with increased heat treatment temperature. A coarse microstructure with a large austenite spacing was found to promote higher fractions of nitride precipitation while nitrogen content was found to affect the amount of precipitation in less extent. The intragranular nitrides cause precipitation hardening in the ferrite and the precipitation was found to be at its most severe in the center of the ferritic regions, with precipitation free zones close to the phase boundaries. The microhardness of the phase was affected accordingly, with increasing hardness towards the center. Charpy v-notch test results show that nitride precipitation causes an embrittlement of the steel while intragranular secondary austenite improves the impact toughness of the material as it shortens the diffusion distance of nitrogen, decreasing the materials susceptibility to intragranular nitride precipitation.

Sammendrag

Intragranulære kromnitrider har skadelig effekt på materialegenskapene til duplex rustfrie stål, men de har ikke blitt viet mye oppmerksomhet frem til nå. Presipitering av nitrider skjer når ferrittfasen blir overmettet av nitrogen og det ikke er tilstrekkelig med tid for diffusjon av nitrogen til austenitt under avkjøling. For å studere materialenes sårbarhet for nitridutfelling ved varierende varmebehandlingstemperaturer, nitrogeninnhold og mikrostruktur ble varmebehandling utført ved temperaturer mellom 1060°C og 1160°C. I tillegg ble det utført mikrohardhetstester og Charpy tester for å undersøke nitridenes effekt på materialegenskapene til stålet. Det finnes ingen standard metode for kvantifisering av nitrider. En ny metode ble derfor introdusert der presipitasjonen ble kvantifisert ved hjelp av arealfraksjon av nitrider i mikroskopibilder. Resultatene viser økt nitridpresipitasjon ved økt varmebehandlingstemperatur. En grov mikrostruktur med stor austenittavstand ble funnet å fremheve preipitasjon av nitrider, mens nitrogeninnhold påvirker nitridutfellingen i mindre grad. Intragranulære nitrider forårsaker presipitasjonsherding i ferritt fasen, og presipitasjonen er mest intens i senter av ferrittregionene med presipitasjonsfrie soner langs fasegrensene. Mikrohardheten av ferritt påvirkes deretter, med økt mikrohardhet inn mot senter. Charpy tester viser at intragranulære nitrider forårsaker forsprøing av stålet, mens intragranulær sekundær austenitt forbedrer duktiliteten ved å korte ned diffusjonsavstanden for nitrogen og gjøre materialet mindre utsatt for nitridutfelling.

Contents

1 Introduction

Duplex stainless steel is commonly used in the offshore oil and gas industry due to their excellent material properties with regards to both strength and corrosion. In 2009, inspections at an oil and gas field revealed a large crack along a weld in a subsea choke module manufactured from 25Cr superduplex stainless steel. Metallographic examination revealed significant intragranular chromium nitride precipitation throughout the thickness of the module leading to embrittlement of the material at low temperatures. Examination of other components of similar type revealed comparable contents of chromium nitride leading to the conclusion that the failed component was not a unique case and that other modules with substandard impact toughness properties most likely had been installed in this specific subsea field [1].

Nitride precipitation is commonly encountered in heavy wall thickness wrought products, but although not an unknown phenomenon it is generally considered less detrimental than the well known intermetallic phases such as σ and χ. Intragranular chromium nitrides and the effects on the mechanical properties in duplex stainless steels have therefore been given little attention compared to the known detrimental effects of intermatallic phases. However, there are now cases revealing problems with material embrittlement related to the presence of chromium nitrides in subsea modules and awareness of the phenomenon should be raised.

Impact toughness testing has proven relatively useful for controlling the quality of duplex stainless steel with respect to intragranular chromium nitride precipitation. Other common methods such as tensile- and hardness tests are however quite insensitive to chromium nitrides and the micrographic examination thus becomes more crucial for quality control. Micrographic examination of duplex stainless steels has commonly been performed after electrolytic etching with 20-40% NaOH/KOH solutions. These methods are inappropriate for revealing the intragranular nitrides, and thus may have been a crucial reason for substandard components previously passing the quality control and the phenomenon not being studied in detail earlier. Metallographic methods capable of detecting chromium nitride precipitates are now being introduced in the industry. The severity of nitride precipitation has in previous works been interpreted qualitatively on a relative scale from 0 to 3. There currently does not exist a standardized method for quantifying the chromium nitride precipitation, nor methods appropriate for inter-laboratory comparisons. There is therefore great need for a reliable micrographic examination for quality control of duplex stainless steels.

This master thesis is a continuation of a previous project work aimed at determining how different parameters affect the intragranular precipitation of chromium nitrides. The parameters previously studied include heat treatment temperature, nitrogen content and austenite spacing as well as a new method of quantification. This thesis expands the investigation to include more duplex alloys than previously tested. The microhardness of the phases will be examined with regards to the amount of nitrides encountered after different heat treatment temperatures. Charpy test results will also be presented to investigate the influence of nitrides on the material toughness and xrd diffraction analysis is carried out to try to verify the presence of chromium nitrides in the microstructure.

2 Theory

Duplex stainless steels are defined as a class of alloys with ferritic-austenitic microstructure, where the components are both stainless. Originally introduced as a low-nickel alternative to austenitic stainless steels the first duplex alloys became commercially available in the 1930s [2]. Considerable efforts have been made to optimize duplex alloys ever since and duplex stainless steels of today generally contain a high alloying content and offer a good combination of weldability and toughness as well as being reasonably economic. The phase determining alloying elements are chromium and nickel which are ferrite - and austenite stabilizing respectively. The typical alloying content of these elements is >20% Cr and 4-8% Ni, varying with each alloy. The alloys classified as superduplex stainless steels typically contain >24% Cr and have a high corrosion resistance expressed in terms of a pitting resistance equivalent (PRE) greater than 40, where PRE = (%Cr + 3.3%Mo + 16%N) [3]. From the phase diagram in Fig.1 it can be seen that the steels have the chemical composition which provides the wanted duplex structure. This microstructure gives the steel unique properties due to the synergistic interaction between the two phases, achieving a result not possibly obtained by the two phases individually. They are well known for a high corrosion resistance and good mechanical strength, and are widely used in harsh environments, such as in the chemical-, paper- and oil and gas industries. Duplex stainless steel products are obtained by several different processes such as casting, forging, extrusion and rolling, and the microstructure and mechanical properties depend on the specific process of fabrication [4]. The complex chemical composition and microstructure render the duplex products sensitive to phase transformations and precipitations that may significantly deteriorate the properties of the material. A thorough knowledge of the connection between microstructure and properties is therefore required to ensure correct production, heat treatment and welding of these steels.

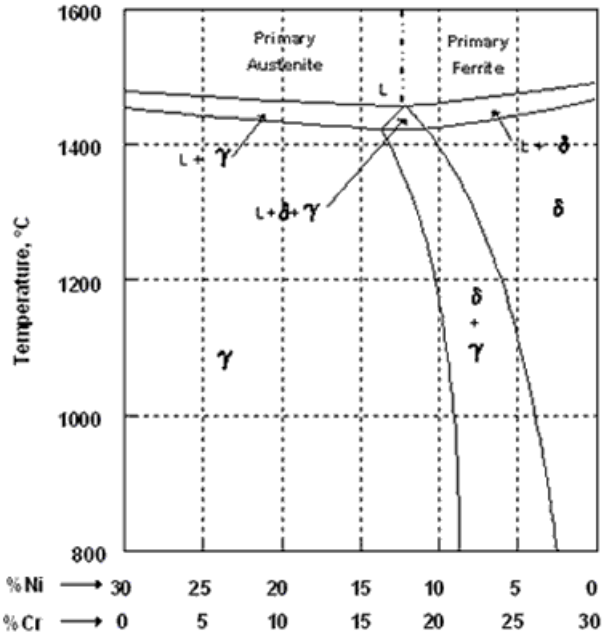

Figure 1: *Phase diagram for duplex stainless steels with wt% Cr and Ni. Duplex structure found with >20%Cr and 4-8%Ni.* [5]

The ideal structure of a duplex stainless steel is a purely ferritic - austenitic structure, with close to equal amounts of each phase and the phase balance obtained is crucial for the mechanical properties [4]. In practice a 50-50 ferrite/austenite microstructure is very difficult to achieve, especially in large dimensions where the cooling rate is challenging to control. Due to the high alloying content the cooling path of a duplex steel contain a high number of obstacles in terms of phase transformation that have to be bypassed in order to avoid unwanted phases and maintain a favourable balance of ferrite and austenite. Most of these precipitation reactions are time and temperature dependent and are indicated in the time-temperature-transformation (TTT) diagram in Fig.2. The effect of alloying elements such as molybdenum and chromium may be observed in the same figure. Although these elements increase corrosion resistance they also expand the time-temperature stability fields of phase transformations and thus increase the tendency in the material to create unwanted intermetallic phases. A sufficiently high cooling rate is therefore crucial to avoid these intermetallic phases. The precipitations also introduce restrictions on the possible temperature range in which duplex steel can be used, as the low temperature precipitation reactions effectively limit the use of duplex alloys to temperatures below approximately 280°C to avoid embrittlement of the material. The deterioration in toughness and corrosion resistance as a result of exposure to high temperatures, is a typical problem to users of duplex steels. The undesirable phases such as intermetallic phases, carbides and nitrides may profoundly affect their properties [6].

In contrast to intermetallic phases and intergranular chromium nitrides, the intragranular nitrides are not proper equilibrium phases and their precipitation kinetics cannot be represented by cooling curves in TTT diagrams. While intermetallic phases tends to be a problem during insufficient cooling, intragranular chromium nitrides behave in an opposite way and are likely to form during rapid cooling. Avoiding the problem of intermetallic phases by rapidly cooling duplex components thus inevitably increases the risk of precipitation of intragranular chromium nitrides.

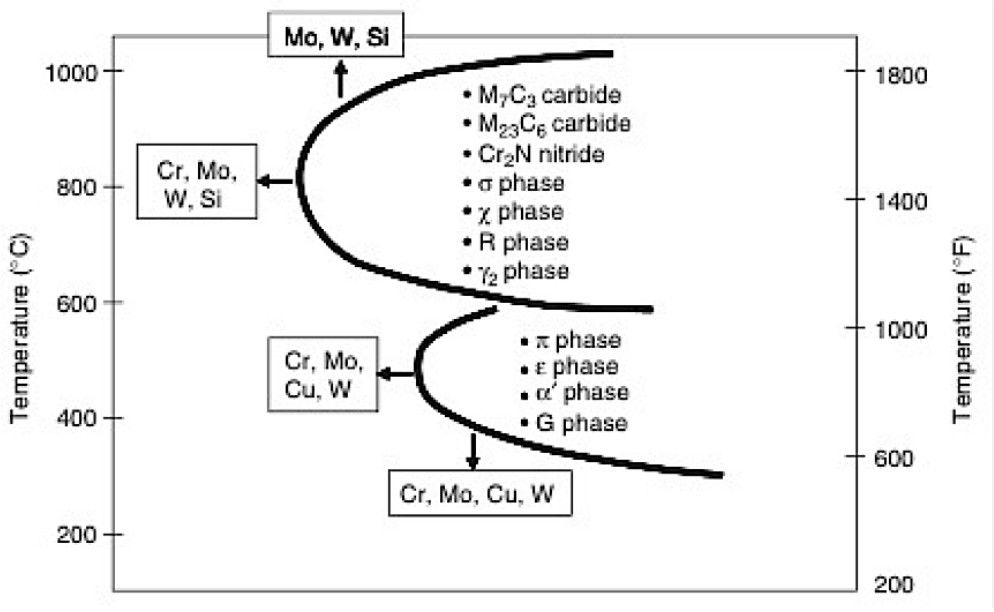

Figure 2: *TTT diagram. Phase transformations and precipitates in duplex stainless steel.Note the effect of alloying elements on the phase transformation fields.* [7]

Modern duplex stainless steels have intentional additions of nitrogen to improve strength and pitting corrosion resistance. In addition the role of nitrogen is to delay the formation of undesired intermetallic phases due to its decreasing effect on the activity of Cr [8]. Nitrogen is also an austenite stabilizing element which is needed to improve the weldability of duplex steels. It plays a crucial part during welding as it helps to control the phase balance in the material. The increased temperature related to the welding procedure leads to zones in the material where the temperature exceeds the ferrite solvus temperature and austenite transforms into ferrite. The transformation of ferrite to austenite upon subsequent cooling depends on diffusion and during rapid cooling the phase equilibrium may not be reached. The weld metal and heat affected zone therefore have a tendency to have a higher ferrite content than the base material. Approximately at least 40% of austenite is required to produce a nitride free weld microstructure in the heat affected zone [9]. Since it occupies interstitial sites in the unit cell, nitrogen has a much faster diffusion than the substitutional elements. It is therefore mobile at lower temperatures and helps to stabilize the austenite. The nitrogen content in duplex steels is in the range of 0.08 - 0.35 wt%, depending on the alloy, well above the solubility limit in ferrite seen in Fig.3 at temperatures below about 1000°C [7]. The addition of nitrogen affects the microstructure of the steel as intragranular nitride precipitation is a consequence of the considerable reduction in nitrogen solubility experienced by the ferritic phase during cooling. This is illustrated in Fig.3 where a significant drop in nitrogen solubility in the ferrite is observed at about 1050 – 1100°C. The redistribution of nitrogen is controlled by diffusion and therefore requires a certain amount of time to be fully completed. Under rapid cooling conditions there is insufficient time for redistribution of nitrogen to austenite leading the ferrite to become supersaturated with nitrogen. The diffusion distance of nitrogen is reduced with the decrease in temperature and becomes much smaller than the dimension of the ferrite grains, leading to nitride precipitation within the ferrite. Only in a narrow zone close to the phase boundary will nitrogen have sufficient time to diffuse into the bordering austenite where the nitrogen solubility is much higher [10].

Interstitially dissolved nitrogen causes a considerable strengthening effect of both the grain interior and the grain boundaries and thus increase the microhardness of both the ferrite and austenite [11][12]. Due to the low solubility limit for nitrogen in high alloyed ferrite (seen in Fig.3), the content of dissolved nitrogen in ferrite is rather small and the two most effective hardening mechanisms in this phase are solid solution hardening due to the substitutional elements and particle hardening from chromium nitrides. A detrimental effect on the scattering of the ferrite microhardness is given by the inhomogeneous distribution of Cr-nitrides, which in turn is affected by the topology of the duplex steel microstructure [11]. Austenite can dissolve about five times more nitrogen than ferrite and therefore experiences solid solution hardening, but no second phase particles can be observed and no particle hardening takes place in the austenitic phase.

Ferrite is usually stronger than austenite and contributes greatly to the tensile properties of the material, but it is less ductile and good toughness properties could therefore be ascribed to the presence of austenite. Because duplex stainless steels often exhibit texture, particularly in the rolled condition, a strong anisotropy of mechanical properties can be expected. This has been shown to lead to values of impact toughness and fracture toughness that are higher in the transverse than in the longitudinal direction relative to the banded structure. Impact toughness has been proven sensitive to precipitation of σ phase even at small amounts [6], but although σ phase appears to be the most deleterious phase other phases such as Cr_2N may contribute to brittle behaviour and in the absence

of σ phase be just as detrimental to toughness [2].

In previous works, [13] [14] [15], large quantities of intragranular chromium nitride rods of the type hexagonal Cr_2N were found which varied in length between approximately 50 and 120 nm with approximately 50 nm thickness. The predominant orientation relationship between the intragranular nitrides and the ferrite matrix was found to be: [16]

$$(110)_\alpha||(0001)_{Cr_2N}$$

$$[\bar{1}11]_\alpha||[\bar{1}101]_{Cr_2N}$$

Thus the most compact planes of both phases are parallel. This orientation relationship which is equivalent to the bcc/hcp Burgers orientation relationship forms a semicoherent interface between the two phases. It has been found in previous studies using transmission electron microscopy [16] that the intragranular nitrides generally exhibit a rodlike morphology. The smaller nitrides were simple rodlike particles, but the larger precipitates often showed a bifurcation at the rod's edges. The rodlike morphology is due to a higher level of coherency of the Cr_2N/α interface along the rod length compared with the tips, which is directly related to the orientation relationship between both phases. The rodlike shape is adopted in order to reduce the overall interfacial energy of the particle [16]. Hence, when the diameter of the precipitate exceeds a certain level, the interfacial energy at the rod tip becomes extremely high, causing the bifurcation. Great amounts of intergranular nitride rods were also observed, with precipitation located along the ferrite grain boundaries and some precipitation along the ferrite/austenite interfaces. The precipitation of chromium nitrides within the ferrite was depleted near the phase boundaries.

The presence of intragranular chromium nitrides may affect the microstructure of duplex stainless steels during heat treatments as they participate in the formation of secondary austenite. Secondary austenite is formed at temperatures below the solution treatment temperature, because the equilibrium volume fraction of austenite will be larger at lower temperatures. Chromium nitrides which precipitates cooperatively are considered to have an indirect effect on the composition of the secondary austenite by accommodating chromium and nitrogen [17]. In a proposed mechanism for secondary austenite formation, chromium nitrides play a double role in the precipitation of secondary austenite [16]. During reheating between 900°C and 1200°C the nitrides will dissolve. Before dissolving they act as nucleation sites for secondary austenite and at the same time the nitrogen liberated upon dissolution provide the nitrogen needed for austenite transformation. A significant intragranular precipitation of secondary austenite may therefore be expected during reheating of duplex steels, especially within the intragranular nitride colonies, either in heat treatment procedures or during multipass welding. The secondary austenite precipitation improves the toughness of the material. However, it has been proposed that the chemical composition of the secondary austenite compromises the corrosion resistance as it generally has lower content of Cr, Mo and N compared to primary austenite. To reduce the differences in chemical composition longer reheating times are needed to allow for austenite homogenization [16].

The presence of intragranular chromium nitrides in the microstructure are detrimental to the material properties. They cause an increase in hardness in the ferrite phase and embrittling of the material [1]. An impaired corrosion resistance of HAZ microstructures with respect to the wrought material has been observed in previous studies [14]. This was in part attributed to the presence of narrow chromium depleted regions around nitrides in the HAZ ferritic grains, which were often observed. Furthermore intragranular nitrides

have shown to have a detrimental effect on pitting corrosion resistance above a certain amount of precipitation due to depletion of Cr and N [4], and there are also concerns related to Hydrogen Induced Stress Cracking (HISC), and the possible influence from nitrides [18].

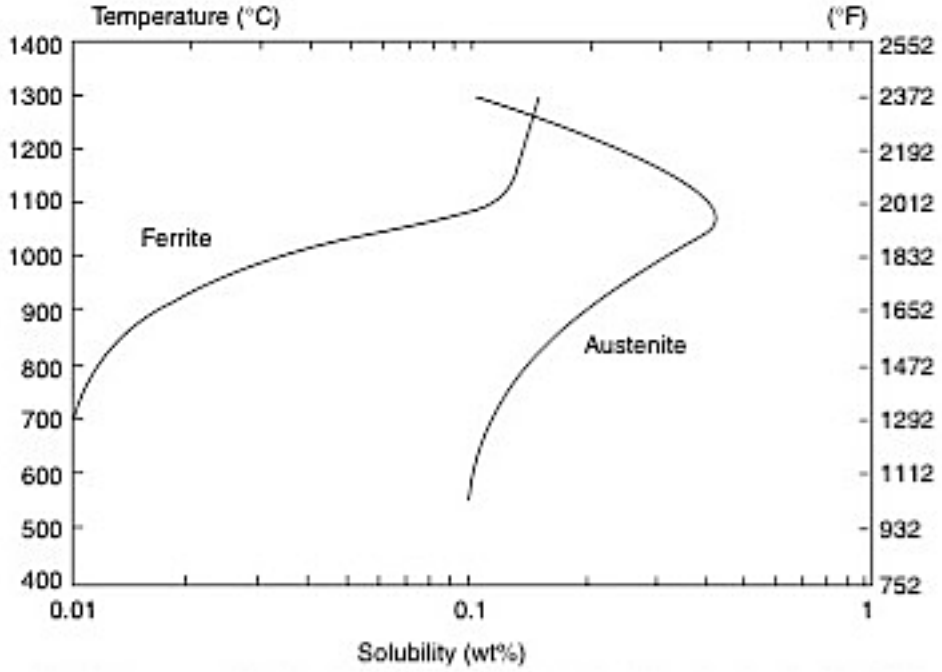

Figure 3: *Nitrogen solubility in ferrite and austenite. Note the rapid reduction of solubility in ferrite as the temperature drops.* [7]

3 Previous work

Chromium nitride precipitation in superduplex stainless steel has not received a great deal of attention and little thorough work has been done covering this subject. However, since the failure of the subsea component was discovered at the Statoil operated oil field, a need for better understanding of the phenomenon has arisen and the interest in the subject has increased. Initial investigation of the failed component was carried out by Statoil and subsequently a student project was carried out by the author covering the phenomenon of intragranular chromium nitrides.

The initial investigation of the failed component performed by Statoil lead to a recommended procedure for metallographic etching involving a two step electrolytic etching procedure to detect chromium nitrides efficiently. The procedure is implemented in this project and described in detail in the section for experimental work. The amount of precipitation observed in the samples was interpreted qualitatively on a relative scale from 0 to 3 where 0.5 is interpreted as minimal precipitation and 3.0 is very severe precipitation. Table 1 shows the results of the water quenched samples heat treated at the three temperatures coinciding with the temperatures used in the present project. Using microhardness testing with the indentations located specifically to the ferrite and austenite phases the investigation revealed that the microhardness of the ferrite seemed to increase in the specimens exhibiting severe chromium nitride precipitation while the microhardness

of the austenite and the overall hardness of the material remained virtually unaffected [1]. The results of the hardness tests are shown in Fig.4 for the samples listed in Table 1. The effect of increased microhardness in the ferrite phase is studied in greater detail in this present project.

Table 1: *Effect of heat treatment temperature on chromium nitride precipitation. Specimens with dimension 30 x 7 x 5 mm held at heat treatment temperature for 30 min and subsequently water quenched (WQ).* [1]

Heat treatment temperature	Cooling	Chromium nitride severity
1060°C	WQ	0.5
1120°C	WQ	2.5
1160°C	WQ	3.0

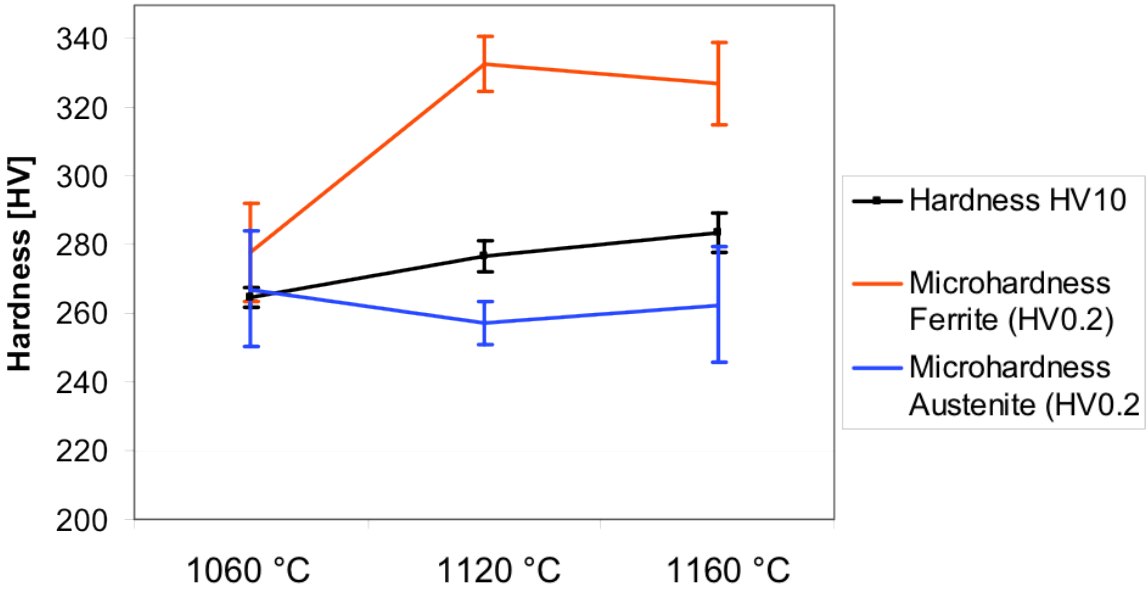

Figure 4: *Results from hardness tests from initial Statoil investigation. Microhardness test performed using 200g load (HV0.2)* [1]

In the previous student project, heat treatments of superduplex stainless steels were performed to study the materials susceptibility to intragranular chromium nitride precipitation. The chemical composition of the materials used in the previous project are listed in Table 2, where material A is the failed subsea component previously investigated by Statoil. All the materials were within the specification of the UNS S32760 alloy standard. The results from the microstructure characterization of the materials are listed in Table 3. All the materials had a relatively coarse grained, forged microstructure with austenite spacing larger than $30\mu m$. Austenite spacing and ferrite bandwidth are terms used alternately in this project. A new method for quantifying nitride precipitation was tested using the two step electrolytic etching procedure recommended by Statoil to reveal etch pits in the ferrite where the material is affected by nitride precipitates, and subsequently quantifying the precipitation by acquiring an estimate of the area fraction of nitrides from micrographs. This method has also been used in this project and is described in detail in the section for experimental work. The quantified nitride fraction results for all the

samples are shown as a function of ferrite bandwidth in Fig.5a to Fig.5f. The parameters believed to influence the materials susceptibility to nitride precipitation and thus investigated in the previous project were heat treatment temperature, microstructure and nitrogen content.

It was found that an increase in heat treatment temperature increases the amount of nitride precipitation. This is due to the nitrogen solubility difference between the ferrite and austenite. The fraction of nitrides was found to increase with increasing width of the ferrite bands. As the austenite spacing increases the diffusion distance for nitrogen becomes larger and more nitrogen remains in the ferrite after cooling of the specimens, resulting in a considerable increase in nitride precipitation. A high nitrogen content revealed a tendency towards a high fraction of nitrides, but it did not seem to affect the amount of nitride precipitation to the same extent as temperature and microstructure.

Table 2: *Chemical composition in wt% of material used in the previous project. Forging ratio added where known.*

Material	**C**	**Si**	**Mn**	**Cr**	**Ni**	**Mo**	**Cu**	**W**	**N**	**Forging Ratio**
A	0,02	0,55	0,50	25,1	6,9	3,7	0,57	0,75	0,27	-
B	0,02	0,42	0,71	25,6	6,4	3,7	0,66	0,57	0,24	-
C	0,02	0,25	0,61	25,39	7,20	3,62	0,55	0,55	0,226	5,45
D	0,02	0,25	0,54	25,6	7,26	3,69	0,55	0,59	0,225	5,01
E	0,02	0,23	0,63	25,3	7,17	3,63	0,53	0,54	0,221	6,16
F	0,02	0,23	0,6	25,53	7,07	3,56	0,55	0,53	0,208	4,5

Table 3: *Mean austenite spacing of the materials investigated in the previous project.*

Material	**%N**	**Mean Aust. spacing** $[\mu m]$	**Stand. dev.** $[\mu m]$	**95% Confidence Interval**
A	0,27	38,0	32,4	[29,7 , 46,1]
B	0,24	33,9	22,8	[28,1 , 39,6]
C	0,226	39,8	28,0	[32,8 , 46,9]
D	0,225	40,1	24,3	[33,9 , 46,2]
E	0,221	30,9	17,3	[26,5 , 35,3]
F	0,208	57,8	41,5	[47,3 , 68,3]

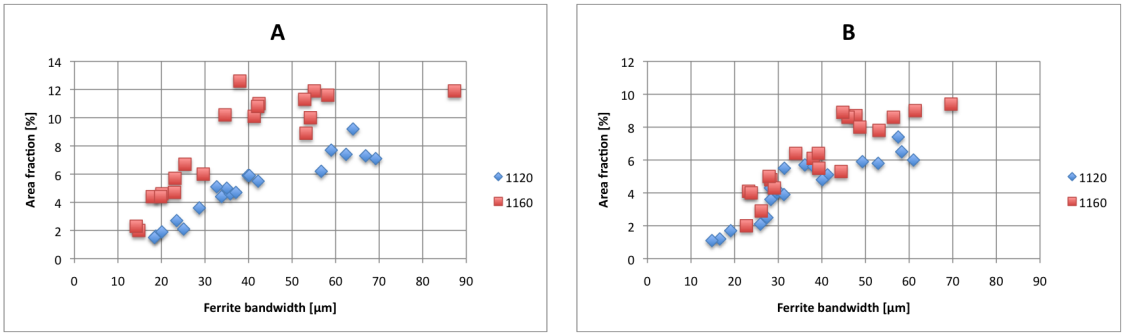

(a) *Sample A*

(b) *Sample B*

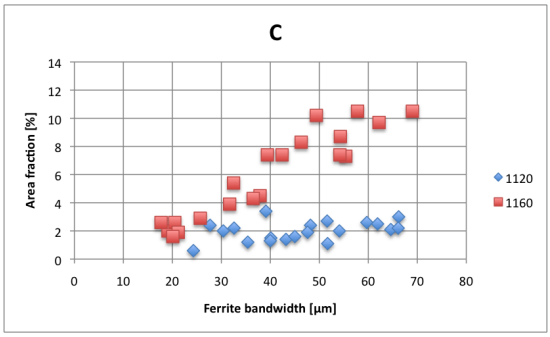

(c) *Sample C*

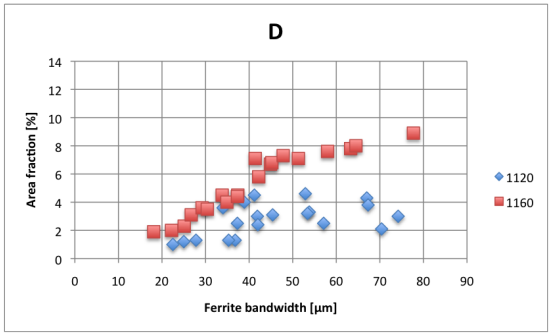

(d) *Sample D*

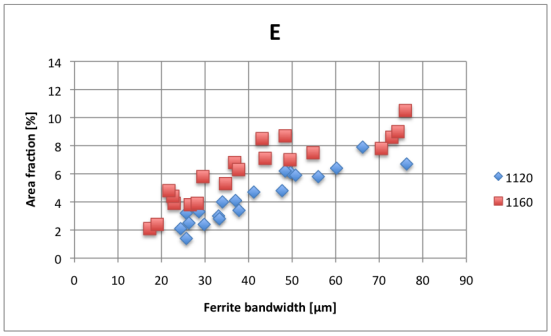

(e) *Sample E*

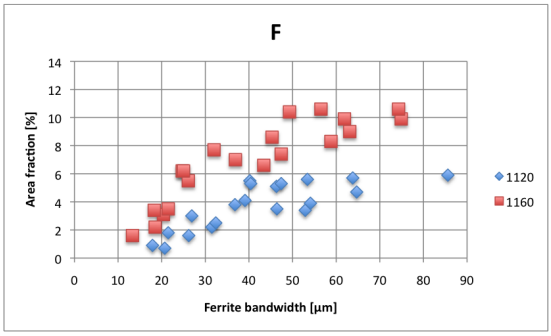

(f) *Sample F*

Figure 5: *Nitride fractions as a function of ferrite bandwidth, i.e austenite spacing, in Samples A to F. Studied in the previous project.*

4 Experimental

The materials used in the heat treatment experiments were superduplex and duplex stainless steels within the specification of the superduplex alloys UNS S32760 and UNS S32750 and the duplex UNS S31803 alloy. The chemical composition of the materials used and their respective UNS standard is given in Table 4.

Table 4: *Chemical composition in wt% of material used. Material 2 and 3 are within the specification of the same alloy, with small differences in chemical composition. Material 4 is a 22Cr duplex alloy.*

Material	**Alloy**	**C**	**Si**	**Mn**	**Cr**	**Ni**	**Mo**	**Cu**	**W**	**N**
1	UNS S32750	0,01	0,38	0,77	25,09	6,98	3,79	0,2	-	0,265
2	UNS S32760	0,02	0,52	0,58	24,92	6,99	3,7	0,57	0,61	0,256
3	UNS S32760	0,02	0,42	0,56	25,04	7,09	3,5	0,58	0,62	0,25
4	UNS S31803	0,02	0,33	1,56	22,39	5,63	3,11	-	-	0,187

4.1 Heat treatment

Specimens were cut using a Discotom Struers cutting machine with 60A25 cut-off wheel for hard ferrous materials to produce samples of the dimension 10x10x30 mm as seen in Fig.6. Heat treatment experiments were performed using a Nabertherm N17/HR furnace with a type-K thermometer controlling the temperature at the specimen placing inside the furnace. The furnace and specimen and thermometer placement are shown in Fig.7a and Fig.7b. Specimens were inserted in a preheated furnace leading to a small drop in temperature at insertion. Timing was therefore delayed until the furnace had reached the desired temperature, approximately 1 min after sample insertion. The heat treatment temperatures used are listed in Table 5 along with the other parameters. Holding time was kept constant at 30 minutes for all specimens and the cooling method used was water immersion quenching (WQ).

Table 5: *Heat treatment parameters.*

Temperature [°C]	**Holding Time** [min]	**Cooling method**
1060	30	WQ
1120	30	WQ
1160	30	WQ

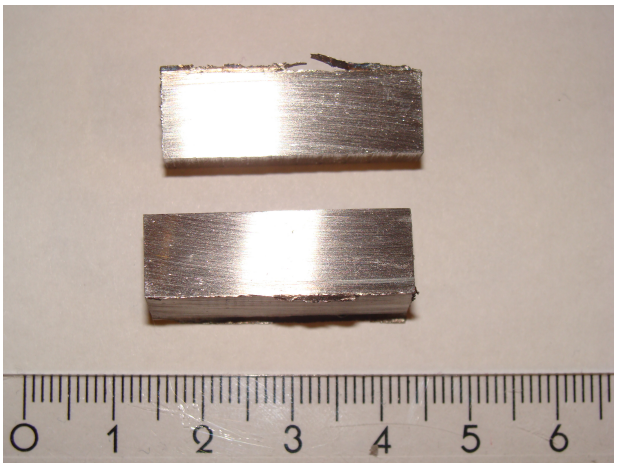

Figure 6: *Samples used in heat treatment experiment. Dimension 30 x 10 x 10 mm.*

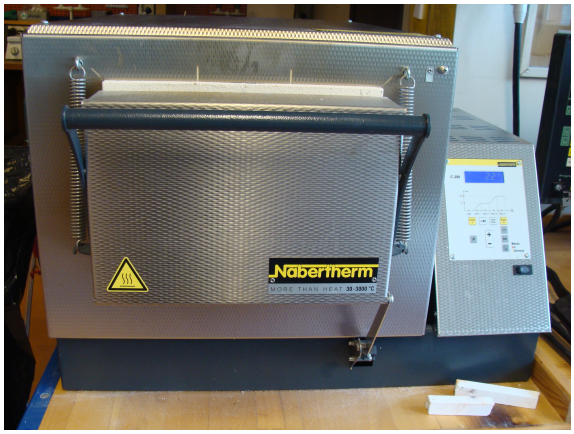

(a) *Naberthern N17/HR furnace*

(b) *Specimen and thermometer positions in the furnace*

Figure 7: *Equipment used in the heat treatment experiments*

4.2 Metallography

Metallographic preparation of specimens included a standard mechanical grinding procedure [19] using stepwise 120-, 320-, 500-, 800- and 1200 grit water cooled silicon carbide (SiC) papers. Specimens were rotated 90° between each step. Specimens were subsequently polished using 6- and 1 μm Struers MD cloths. Two-step electrolytic etching was performed to reveal the microstructure of the samples. The etchants and parameters used in the procedure are listed in Table 6.

Table 6: *Parameters used in the electrolytic etching procedure*

	Etchant	**Voltage** [V]	**Time** [s]	**Application**
Step 1	10% oxalic acid	5	8	Delineates microstructure. Poor contrast between phases
Step 2	20% NaOH	2	6	Colours ferrite and intermetallic phases

The oxalic acid is documented to be successful in delineating intragranular chromium nitride precipitates by revealing a high density of small etching pits in the ferrite phase where the material is affected by nitride precipitates. It is therefore a method that although not making them directly visible provides indirect evidence for the presence of intragranular nitrides [1]. The second step in the etching procedure provide a good contrast between the individual phases in the specimen, thus facilitating subsequent microstructure analysis in a microscope.

4.3 Quantification

The microstructure was observed and imaged using a Leica MEF4M light microscope with Jenoptik Laser Optik Systeme camera type ProgRes C10 plus. The instrument is shown in Fig.8. The samples came from forged products and an anisotropic microstructure was therefore expected since forging results in elongated domains of ferrite and austenite in the forging direction. The samples were prepared and imaged in two directions in order to identify the optimal direction for investigation of chromium nitrides. The microstructures in the two directions are shown in Fig.9a and 9b. The elongated microstructure was chosen for this project.

A study of the microstructure of the material as received was performed prior to heat treatment. The mean austenite spacing of the samples was measured using the line intercept method as recommended in the DNV standard for design of duplex stainless steel subsea equipment exposed to cathodic protection [20]. Measurements were performed by superimposing a straight line over the sample in the microscope and measuring the length of the line falling within the ferrite phase using a Sony LH51 displacement measuring unit. The measurements were carried out in four different random fields on each specimen and the total number of measurements were 60.
The standard deviation was calculated using Equation 1 and a confidence interval of 95% was calculated using Equation 2. Where X_i is the individual measurements, $\overline{X}$ is the

mean austenite spacing and n is the total number of measurements.

$$s = \left[\frac{\Sigma(X_i - \overline{X})^2}{n-1}\right]^{\frac{1}{2}} \tag{1}$$

$$\overline{X} \pm 1,96\left(\frac{s}{\sqrt{n}}\right) \tag{2}$$

Figure 8: *Leica MEF4M light microscope and Sony LH51 displacement measuring unit.*

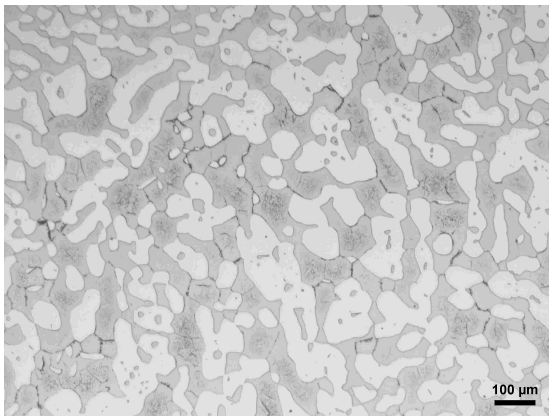

(a) *Micrograph of equiaxed microstructure in sample B.*

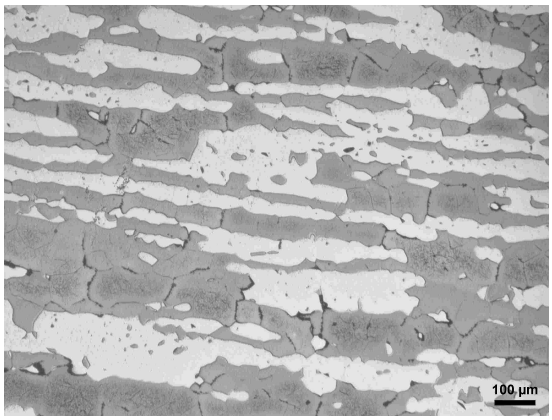

(b) *Micrograph of elongated microstructure in sample B.*

Figure 9: *Micrographs showing the anisotropy in the microstructure of forged components.*

In order to quantify the nitride content based on variation in microstructure twenty micrographs of ferrite bands with different bandwidths were recorded of each sample. The

contrast in the images was later configured digitally to ensure maximum contrast between nitride precipitates and the ferrite phase. This was done to facilitate the study of area phase fractions by the means of the computer software program "Image Access Easy Lab", which separates phases on the basis of the contrast between them. This is illustrated in Fig.10. By means of this software the ferrite bandwidth was measured and the area fraction of etching pits was quantified. This result will be presented as the area fraction of nitrides as the etching pits are an indirect measure of nitride precipitation. The results were later plotted as a function of ferrite bandwidth. Precipitation decreases towards the phase boundaries, the areas chosen for inspection were therefore approximately in the center of each ferrite band where precipitation is at its most severe.

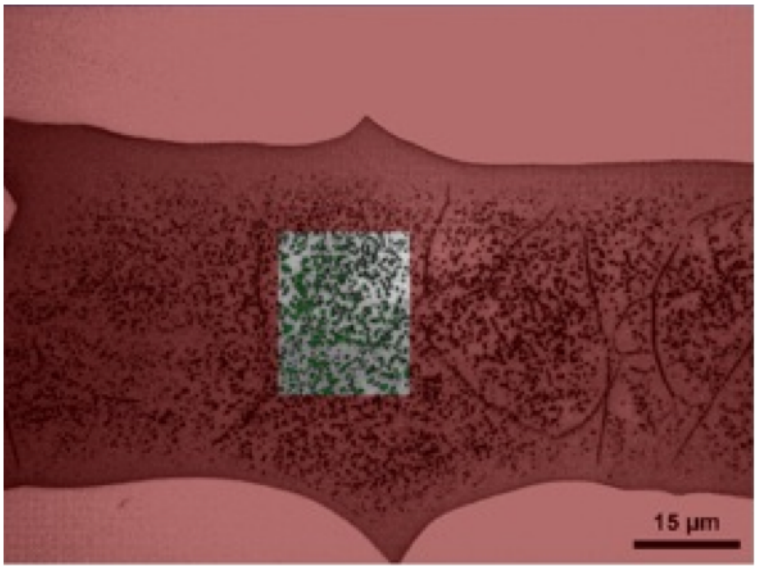

Figure 10: *Screenshot illustrating the use of Image Access Easy Lab software program. Highlighted area is the inspected area of the ferrite band. Particles counted are colored green. The bright areas surrounding the ferrite band are austenite, showing no sign of nitride precipitation.*

4.4 Microhardness

Microhardness testing was performed using the instrument Leica VMHT MOT Vickers microhardness tester. The alloys investigated in the previous project were included in the hardness tests and the chemical composition of these alloys is listed in Table 2. In order to distinguish between the two phases the samples were etched with 20% NaOH prior to testing as this colours the ferrite phase but renders the hardness of the material unaffected. Indentations were placed specifically within the ferrite and austenite phases and carried out according to standard procedures for Vickers microhardness testing [21]. A total of 15 indentations were taken in each phase using a load of 200gf and a indentation duration of 10s. The indentations were taken in the center of the ferrite bands where precipitation is most severe and the hardness should be most affected. The instrument used is shown in Fig.11. In addition a hardness profile of the ferrite bands of some of the alloys was investigated taking indentations across a ferrite band with a load of 25gf.

Figure 11: *Leica microhardness tester.*

4.5 Charpy test

Charpy impact specimens were machined from a forged superduplex component. The chemical composition of the material is given in Table 7. The specimens were cut in the longitudinal direction of the component and were standard v-notch Charpy specimens of dimensions 10 x 10 x 55 mm as seen in Fig.12. The testing machine and specimen arrangement is shown in Fig.13. Charpy tests were performed on samples heat treated at 1120°C and 1160°C as well as samples not heat treated used as reference material. A series of three specimens were tested for each temperature. The impact test was carried out at -46°C on a Zwick charpy test machine with a 300J hammer. The samples were held in a cooling bath for 15 minutes prior to testing according to standard procedures.

Table 7: *Chemical composition in wt% of material used in charpy test. The exact nitrogen content is not known.*

Material	C	Si	Mn	Cr	Ni	Mo	Cu	W	Al	N
UNS S32760	0,02	0,31	0,52	24,81	7,08	3,59	0,59	0,57	0,011	<0,24

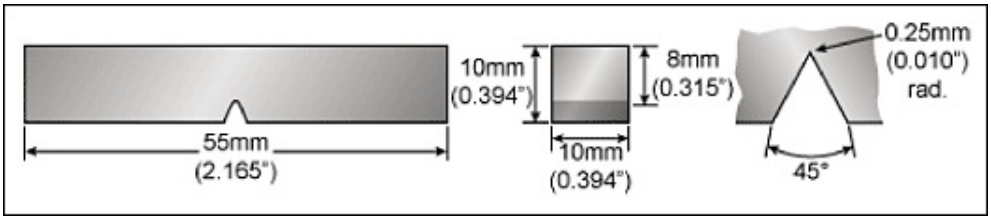

Figure 12: *Charpy v-notch specimen dimensions.*[22]

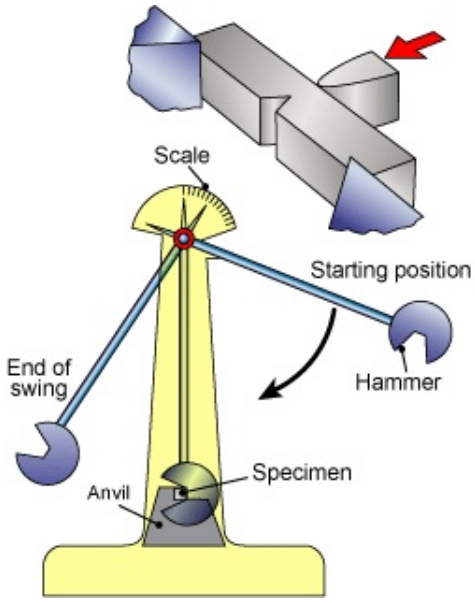

Figure 13: *Charpy testing machine and specimen arrangement.*[22]

4.6 XRD

Diffraction analysis was performed on material A, heat treated at 1160°C. The analysis was performed on Siemens D5005 X-ray diffractometer. The input parameters used are listed in Table 8.

Diffraction analysis was done by using the software Diffracplus XRD Commander and the quantitative Rietveld analysis of the experimental results were done with the software DiffracEVA.

Data was collected with CuKα-rays in the area $35° \leq 2\theta \leq 100°$ with a step interval of 0.04°. The scanned area of the sample was constant making the slit openings variable during the scan depending on angle of the incoming beam.

Table 8: *Input parameters for Diffrac plus XRD Commander for the XRD analysis*

Analysis parameters	
Current	40 mA
Voltage	40 kV
Divergence slit	v6.60
Antiscattering slit	v6.60
Step size	0.04 °
Time per step	14 sec
Total scan time	6h 19 min

5 Results

5.1 Microstructure characterization

The material was studied as received to characterize the original microstructure. The mean austenite spacing was measured for each alloy and the results are listed in Table 9 with calculated standard deviation and confidence interval. All materials have a mean austenite spacing greater than $30\mu m$ and can be classified as having relatively coarse microstructure according to the DNV standard for duplex stainless steel subsea equipment [20]. A high degree of variation in microstructure was observed leading to quite large deviations in the measurements. The superduplex alloys showed some signs of nitride precipitation in the as received condition while the duplex alloy showed no sign of chromium nitrides before the heat treatment experiments. Micrographs showing the original microstructures are included in Fig.14a to 14d on page 20.

Table 9: *Mean austenite spacing of the materials used.*

Material	**%N**	**Mean Aust. spacing** $[\mu m]$	**Stand.dev.** $[\mu m]$	**95% Confidence Interval**
1	0,265	45,6	34,1	[36,9 , 54,2]
2	0,256	59,9	35,1	[51,1 , 68,8]
3	0,25	65,4	37,8	[55,8 , 74,9]
4	0,187	40,5	27,1	[33,7 , 47,4]

5.2 Heat treatment

The influence of heat treatment temperature on intragranular precipitation was investigated by heating samples of equal dimensions (Fig.6) to three different temperatures followed by immediate water quenching. The holding time was kept constant at 30 minutes for all samples, and the temperatures used were within the range of 1060 - 1160°C. For comparison, the standard heat treatment temperature for UNS S32760 superduplex stainless steel is 1100 - 1140°C. Micrographs showing the resulting microstructures in the samples are shown in Fig.15a to 17d on page 21. The micrographs show close to no precipitation in samples heat treated at 1060°C. The precipitation in these samples are therefore not quantified. Significant precipitation is observed in samples heat treated at 1120°C and samples heat treated at 1160°C show severe precipitation. The grain boundaries within the ferrite bands are not observed in samples without nitride precipitation. They are however clearly visible with precipitation present in the ferrite. Nitrides thus seem to form on the grain boundaries as well as within the grains. The nitrides located at grain boundaries are not accounted for when quantifying the nitride precipitation in this project. A narrow zone without precipitation is observed along the phase boundary of ferrite and austenite. In Fig.17a a precipitation free zone may also be observed along the grain boundary within the ferrite. This phenomenon is not observed in Fig.17b where the boundaries observed are believed to belong to cellular substructures in the ferrite. In Fig.17c both type of boundaries are observed within the same ferrite region with a clearly visible precipitation free zone lies along the grain boundaries and no such zone appearing along the other boundaries.

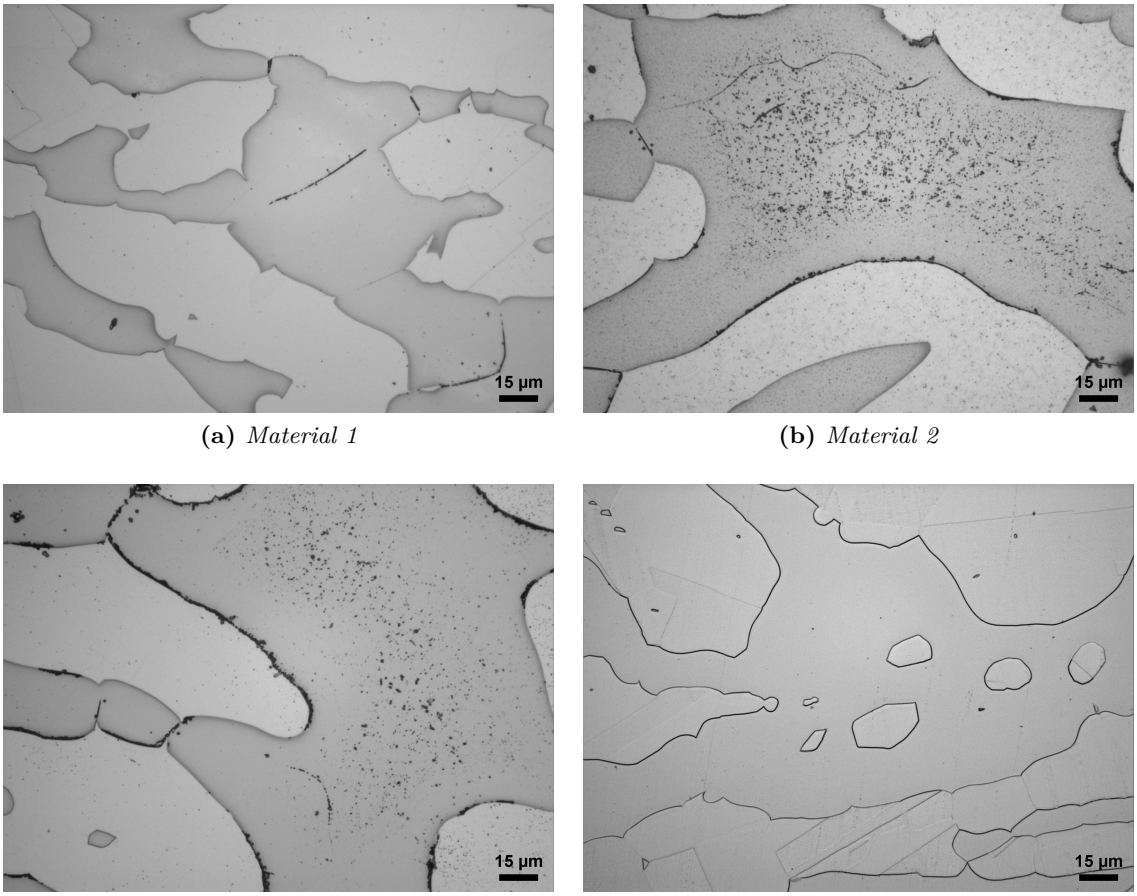

(a) *Material 1*

(b) *Material 2*

(c) *Material 3*

(d) *Material 4*

Figure 14: *Micrographs showing microstructure of the different materials as received. Ferrite has the darkest colour, while intragranular precipitates appear as black dots inside the ferrite.*

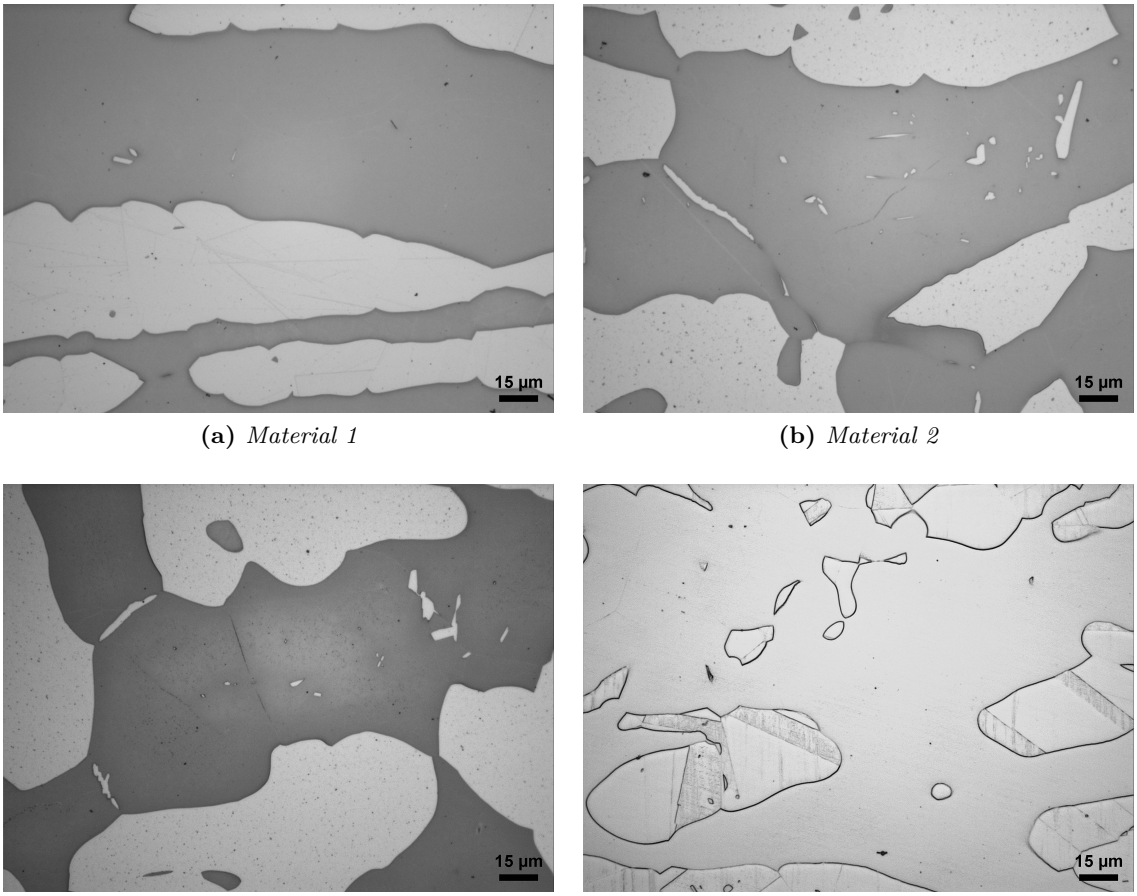

(a) *Material 1*

(b) *Material 2*

(c) *Material 3*

(d) *Material 4*

Figure 15: *Micrographs showing microstructure of the different materials heat treated at 1060° C. No precipitation of intragranular nitrides is observed nor are the grain boundaries visible.*

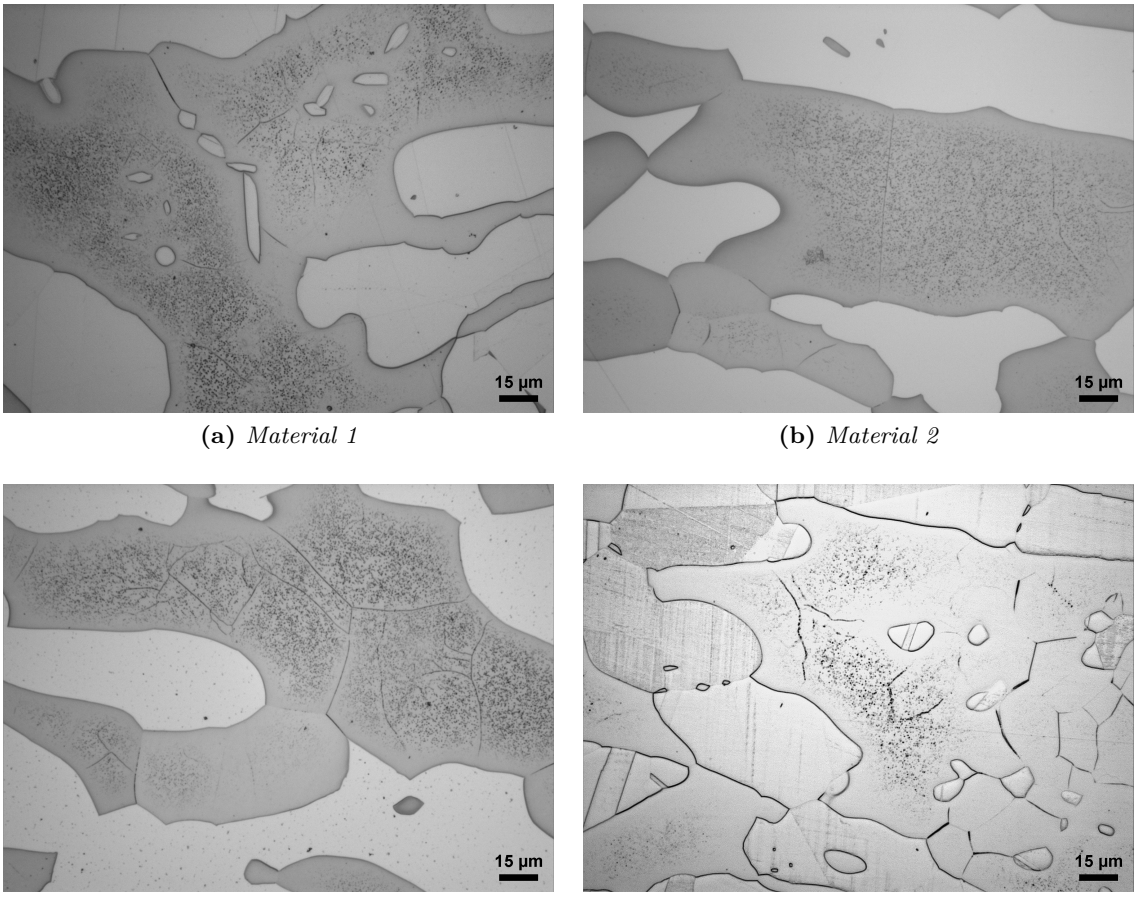

(a) *Material 1*

(b) *Material 2*

(c) *Material 3*

(d) *Material 4*

Figure 16: *Micrographs showing microstructure of the different materials heat treated at 1120° C. Intense precipitation of intragranular nitrides observed in the ferrite. A precipitation free zone is observed along the phase boundaries.*

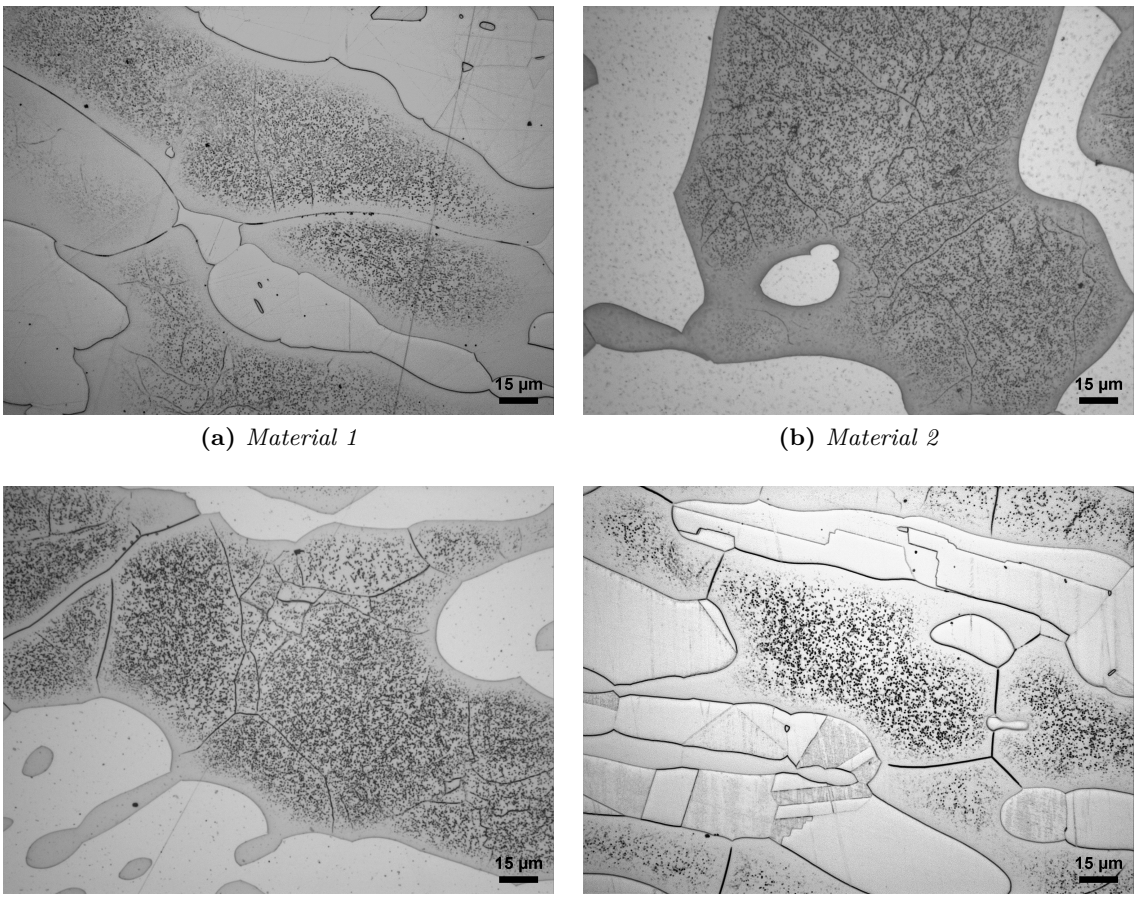

(a) *Material 1*

(b) *Material 2*

(c) *Material 3*

(d) *Material 4*

Figure 17: *Micrographs showing microstructure of the different materials heat treated at 1160° C. Severe precipitation of intragranular nitrides observed in the ferrite. Precipitation free zones are observed along phase boundaries and grain boundaries.*

To investigate the effect of microstructure on intragranular precipitation the fraction of nitrides obtained by the use of Image Access Easy lab was plotted as a function of ferrite bandwidth. The numbers obtained by the software are listed in appendix A. The results show a high correlation between increased nitride precipitation and increased ferrite bandwidth as can be seen in Fig.18a to Fig.19b. The effect of heat treatment temperature is shown in the same figures as the fraction of nitrides increase with increased temperature.

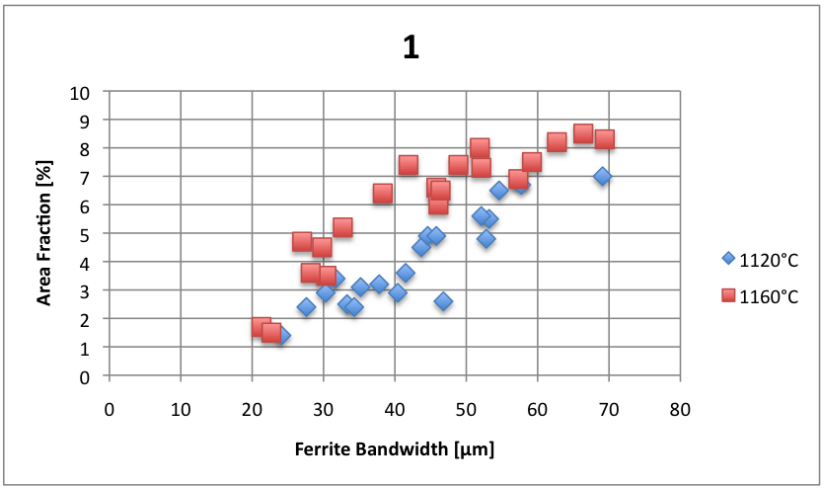

(a) *Nitride fraction in material 1*

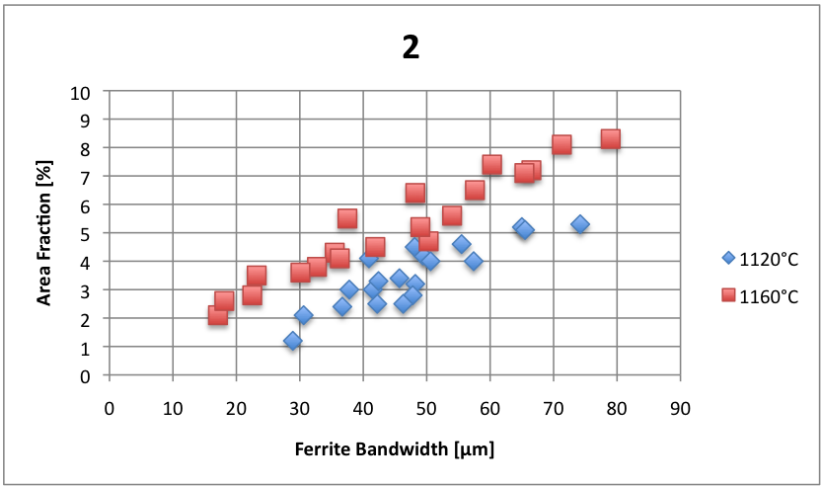

(b) *Nitride fraction material 2*

Figure 18: *Graphs showing the effect of microstructure and increasing heat treatment temperature on nitride fraction in the various specimens.*

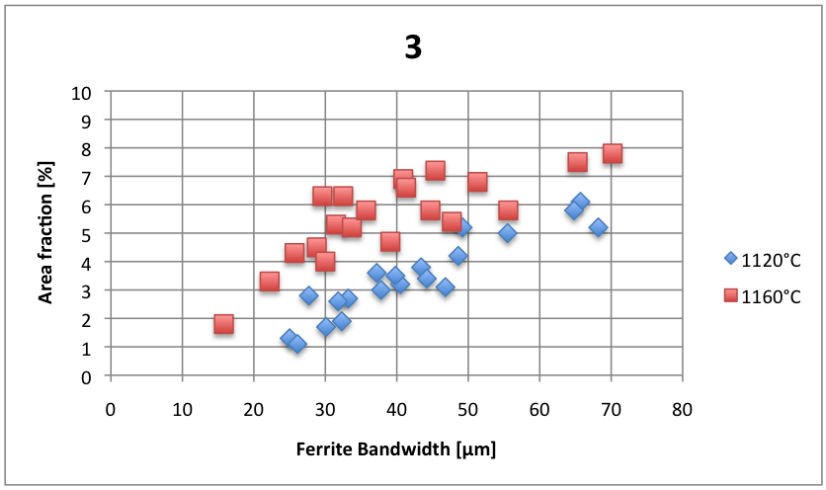

(a) *Nitride fraction in material 3*

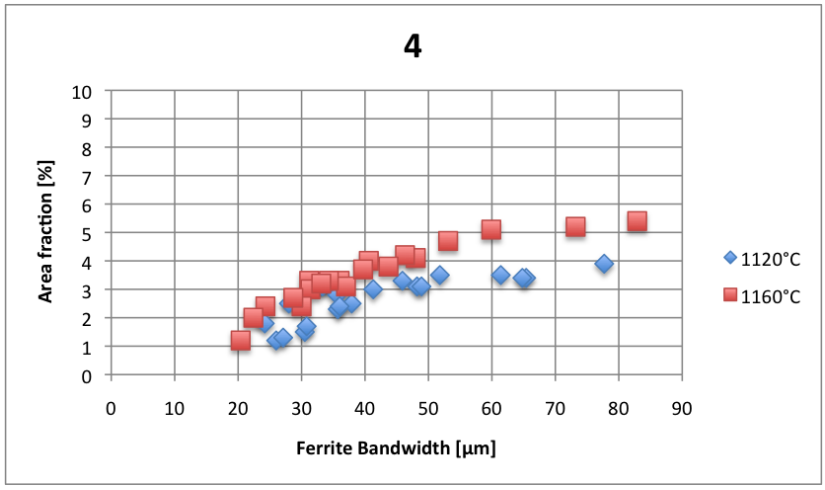

(b) *Nitride fraction in material 4*

Figure 19: *Graphs showing the effect of microstructure and increasing heat treatment temperature on nitride fraction in the various specimens.*

To observe the effect of nitrogen content on nitride precipitation the results of the samples were compared against each other and to the results of sample A obtained in a previous project. The results are shown in Fig.20a and Fig.20b for the samples heat treated at 1120°C and 1160°C respectively. The fraction of precipitates of all the alloys studied in the previous project are shown in Fig.5a to 5f on page 11. There are small differences in nitrogen content in the superduplex alloys and as expected overlapping results were found when comparing the nitride fractions. The duplex alloy differ the most from the other alloys with regards to chemical composition but this sample also reveal overlapping results. In thin ferrite bands the nitrogen content thus seem to have little effect on the fraction of nitrides. However, in broader ferrite bands and at higher temperature the results differ more, with the duplex alloy containing the least amount of nitrogen containing an overall lower fraction of precipitates and Material A containing the most amount of nitrogen presenting the highest fraction of precipitates.

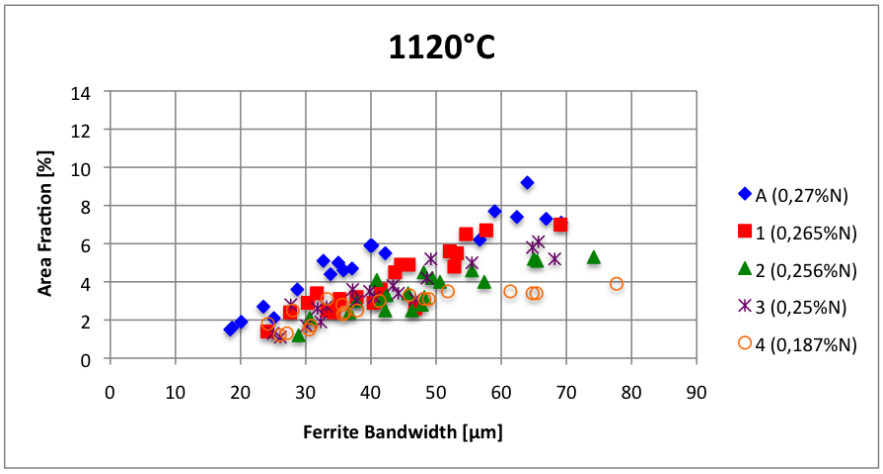

(a) *Ferrite bandwidth vs. area fraction of nitrides in different alloys heat treated at 1120° C*

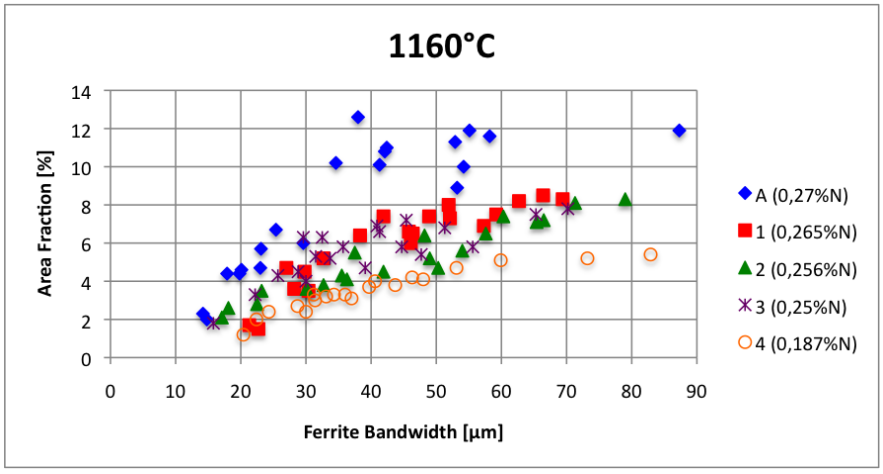

(b) *Ferrite bandwidth vs. area fraction of nitrides in different alloys heat treated at 1160° C*

Figure 20: *Graphs showing the effect of different nitrogen content on nitride precipitation. The results for sample A were obtained in a previous project.*

5.3 Microhardness

Microhardness indentations were taken to study the nitrides effect on the hardness of the material. The samples include the 6 materials characterized in the previous project as well as the 4 alloys investigated in this project. 15 indentations were taken in each of the two phases separately with a load of 200gf. The results of the individual indentations are listed in Appendix B. The average hardness results for both phases in the as received condition and all heat treatment conditions are listed in Table 10. The results were plotted and are shown in Fig.21a to Fig.24b with standard deviations and maximum hardness values in ferrite added. As chromium nitride precipitation takes place in the ferrite phase in superduplex stainless steels the hardness of the austenite is left essentially unaffected by the heat treatment and subsequent water quenching. An increased hardness is observed in the ferrite phase as the heat treatment temperature is increased, consistent with the increased amount of nitride precipitation occurring in these samples. The samples showed a significant increase in hardness, ranging between 8–18%, when comparing between heat treatment temperatures of 1060°C and 1160°C. The increase in hardness is lower comparing between 1120°C and 1160°C, with an increase between 1-5% in the samples, with some even showing a slight decline in hardness at 1160°C. The individual maximum hardness values obtained in the ferrite are much larger than the average value of the samples showing the large deviations in microhardness existing in the samples.

Table 10: *Average microhardness [HV] of the phases in the as received condition and after the different heat treatment temperatures.*

Sample	As Received		1060°C		1120°C		1160°C	
	Ferrite	Austenite	Ferrite	Austenite	Ferrite	Austenite	Ferrite	Austenite
1	296	270	309	277	346	284	349	279
2	313	267	318	268	347	269	356	274
3	316	266	317	265	360	279	368	268
4	252	245	278	259	308	268	300	259
A	282	265	300	272	317	283	326	276
B	298	280	294	273	328	278	326	276
C	301	275	304	276	322	280	339	267
D	293	264	307	264	354	280	364	279
E	348	289	344	302	372	299	389	318
F	299	266	327	255	354	263	357	259

The ferrite bandwidth where the indentations were taken was measured and the hardness was plotted as a function of this bandwidth for the samples heat treated at 1120°C and 1160°C. The results are shown in Fig.25a to Fig.28b on page 32. It has previously been shown that a strong correlation between nitride precipitation and ferrite bandwidth exist. It was therefore expected an increased hardness with increased bandwidth as a higher amount of precipitates is expected to form in the broader ferrite bands at these heat treatment temperatures.

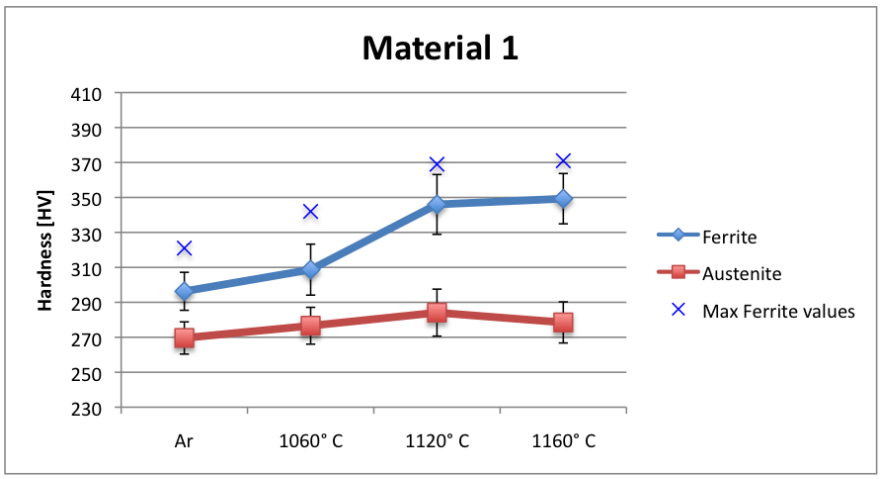

(a) *Microhardness of material 1*

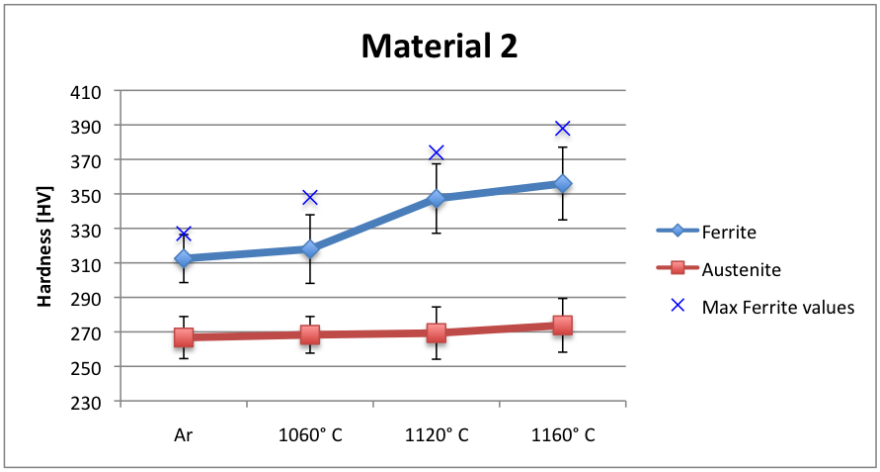

(b) *Microhardness of material 2*

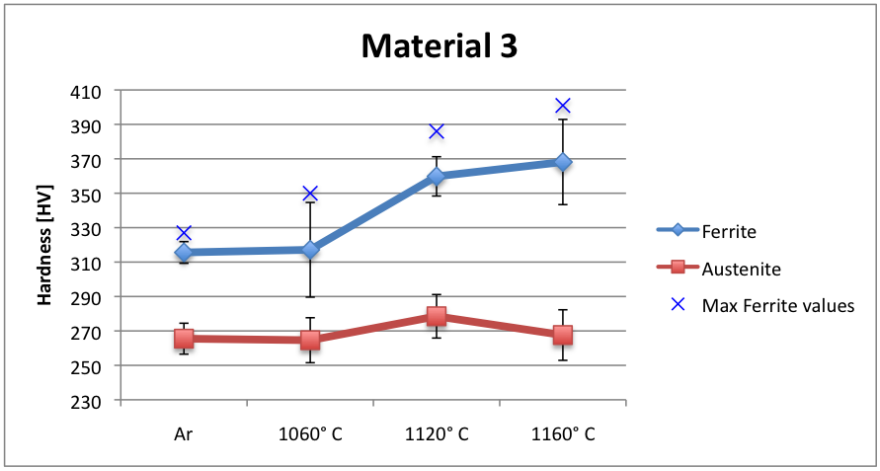

(c) *Microhardness of material 3*

Figure 21: *Graphs showing the average microhardness of the various specimens and maximum hardness values in ferrite. Standard deviation indicated by error bars.*

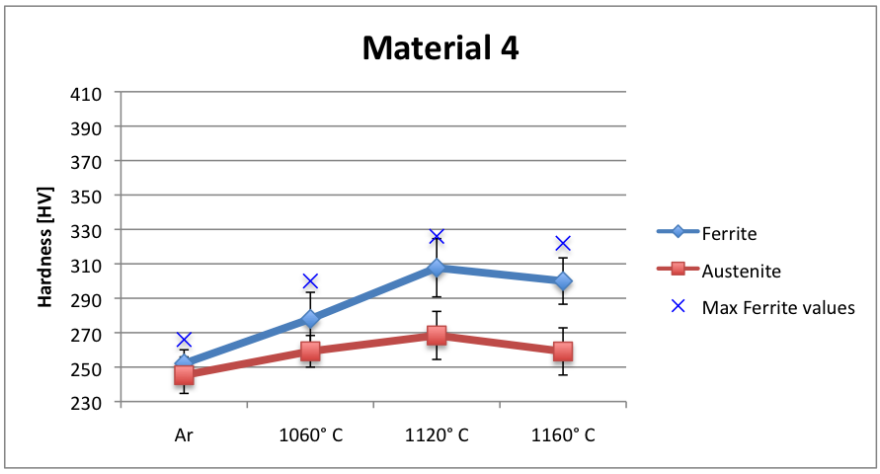

(a) *Microhardness of material 4*

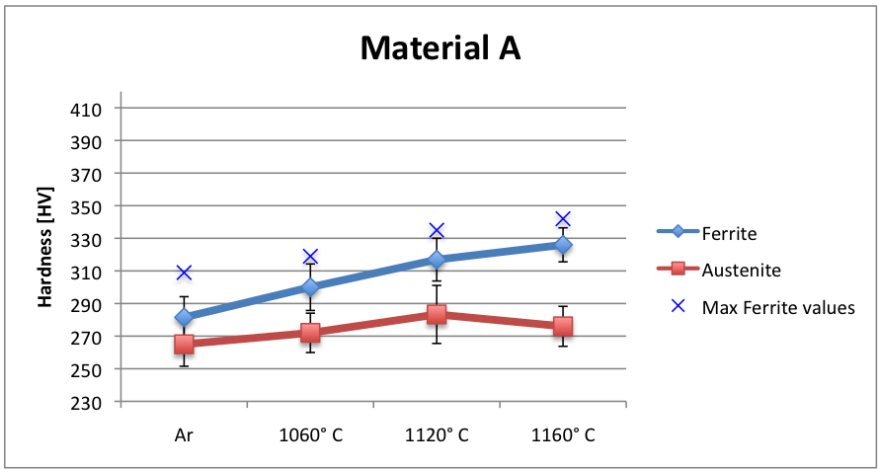

(b) *Microhardness of material A*

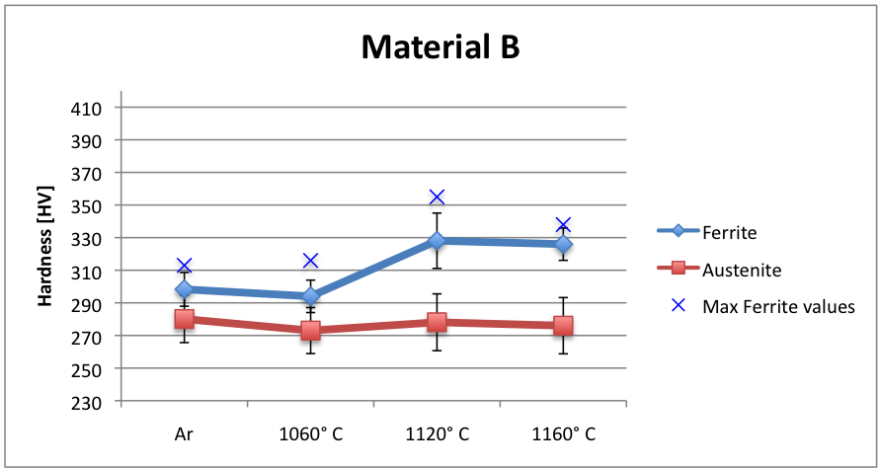

(c) *Microhardness of material B*

Figure 22: *Graphs showing the average microhardness of the various specimens and maximum hardness values in ferrite. Standard deviation indicated by error bars.*

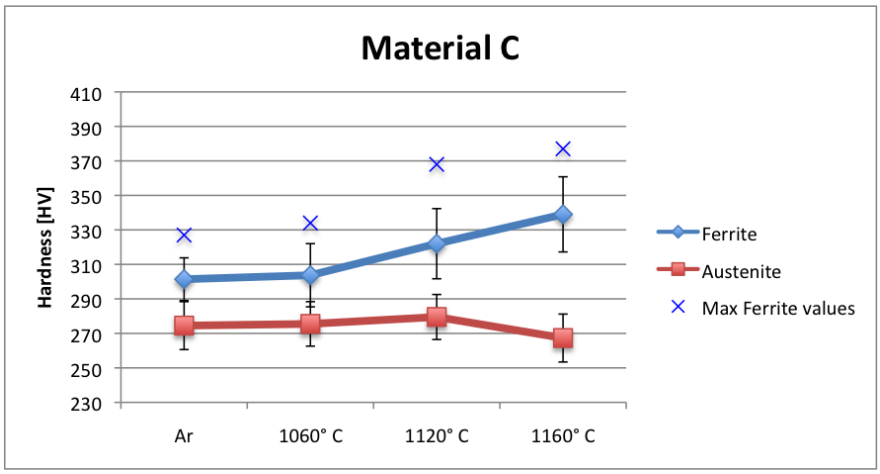

(a) *Microhardness of material C*

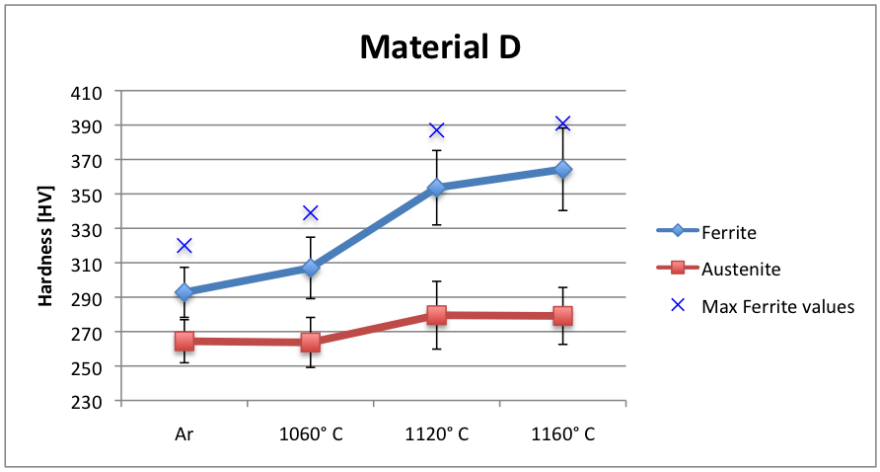

(b) *Microhardness of material D*

Figure 23: *Graphs showing the average microhardness of the various specimens and maximum hardness values in ferrite. Standard deviation indicated by error bars.*

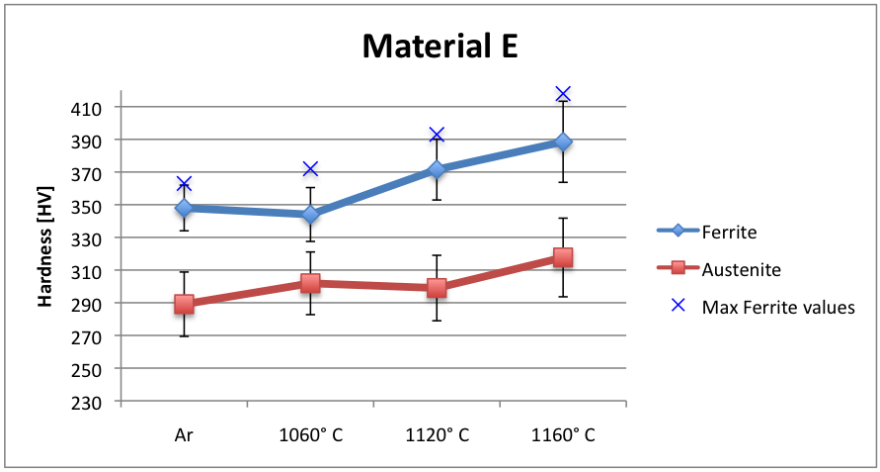

(a) *Microhardness of material E*

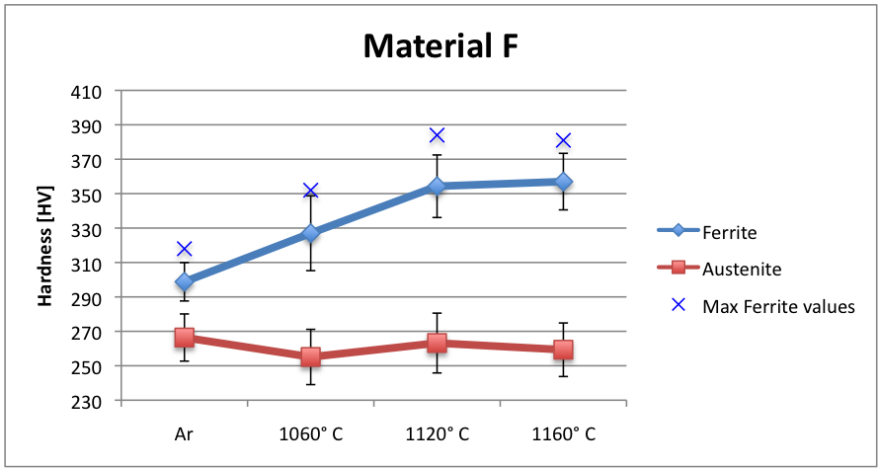

(b) *Microhardness of material F*

Figure 24: *Graphs showing the average microhardness of the various specimens and maximum hardness values in ferrite. Standard deviation indicated by error bars.*

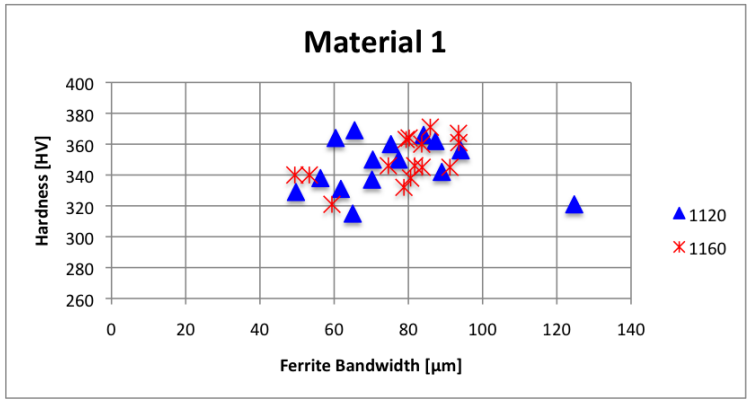

(a) *Microhardness of ferrite in sample 1.*

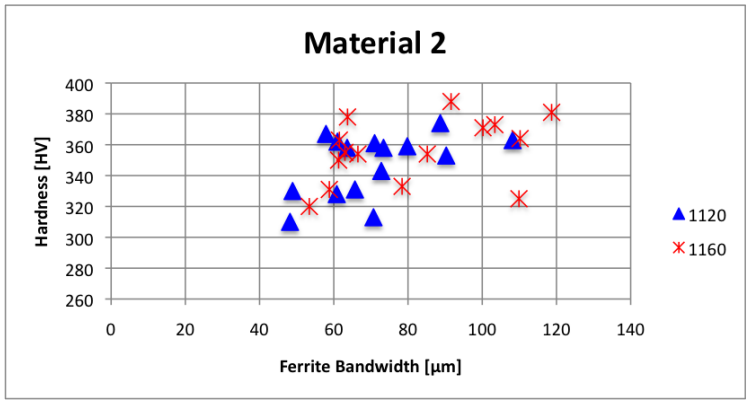

(b) *Microhardness of ferrite in sample 2.*

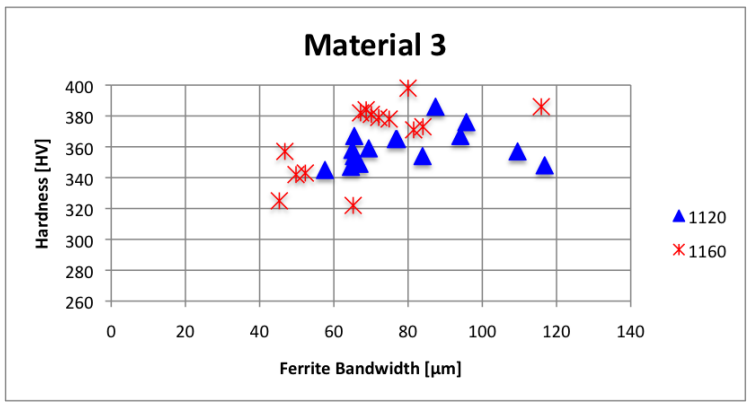

(c) *Microhardness of ferrite in sample 3.*

Figure 25: *Microhardness as a function of ferrite bandwidth in samples heat treated at 1120° C and 1160° C. 15 indentations were taken in each sample for the two different heat treatment temperatures.*

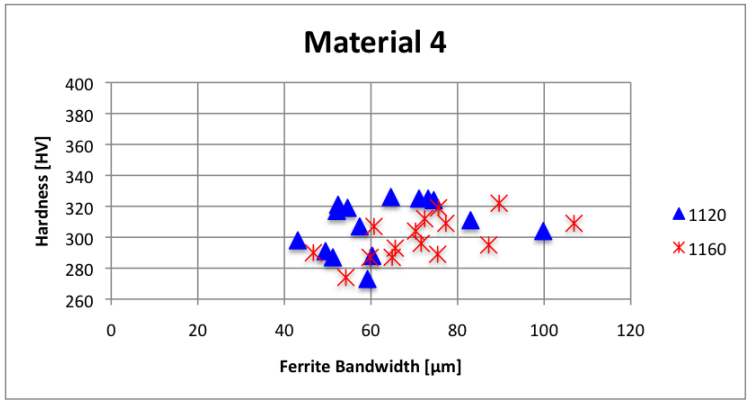

(a) *Microhardness of ferrite in sample 4.*

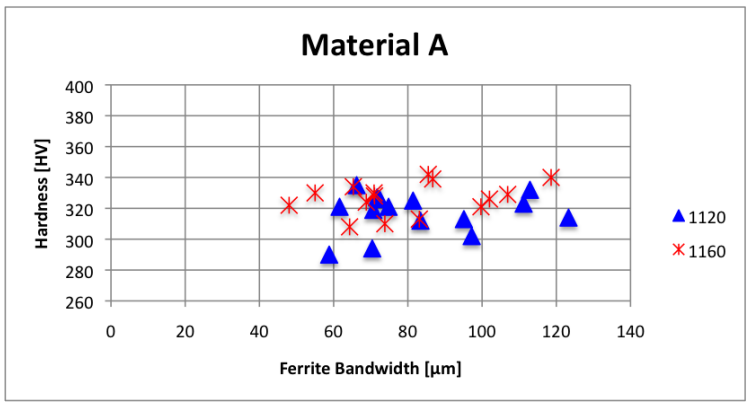

(b) *Microhardness of ferrite in sample A.*

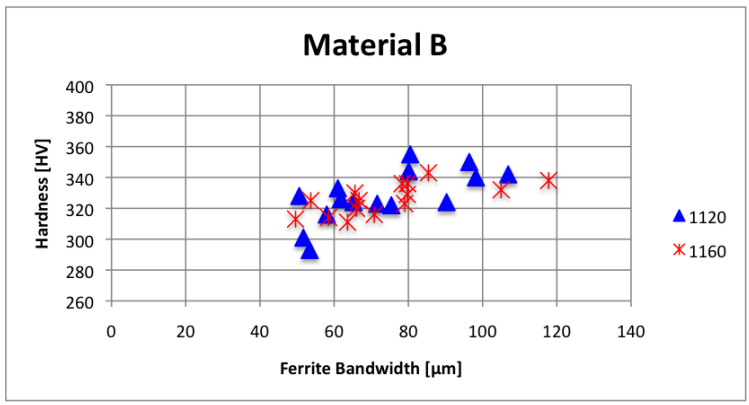

(c) *Microhardness of ferrite in sample B.*

Figure 26: *Microhardness as a function of ferrite bandwidth in samples heat treated at 1120° C and 1160° C. 15 indentations were taken in each sample for the two different heat treatment temperatures.*

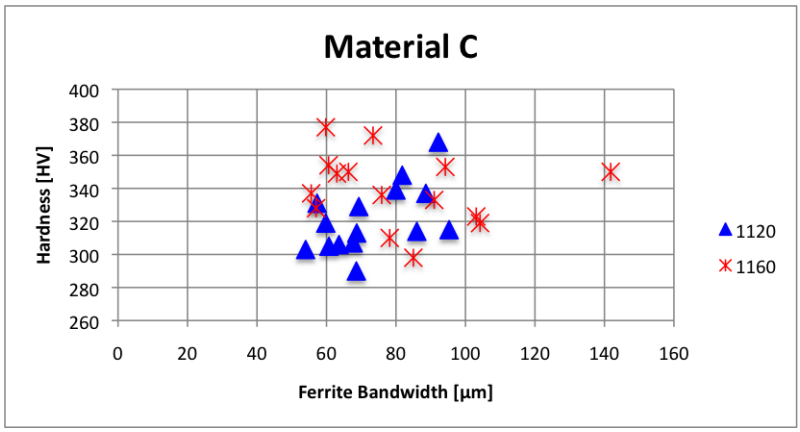

(a) *Microhardness of ferrite in sample C.*

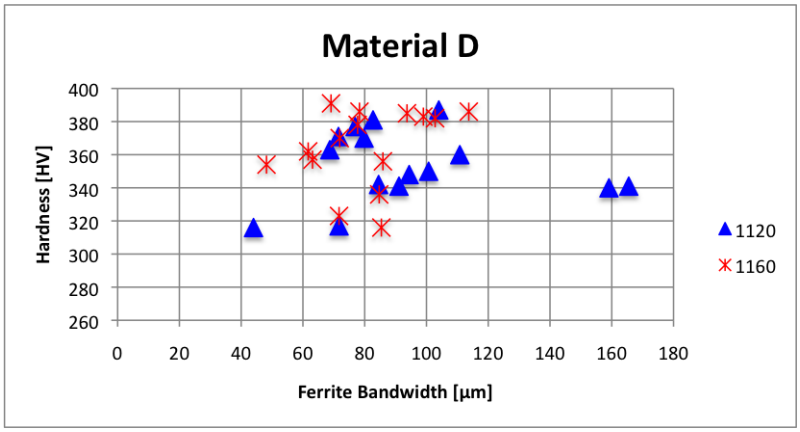

(b) *Microhardness of ferrite in sample D.*

Figure 27: *Microhardness as a function of ferrite bandwidth in samples heat treated at 1120° C and 1160° C. 15 indentations were taken in each sample for the two different heat treatment temperatures.*

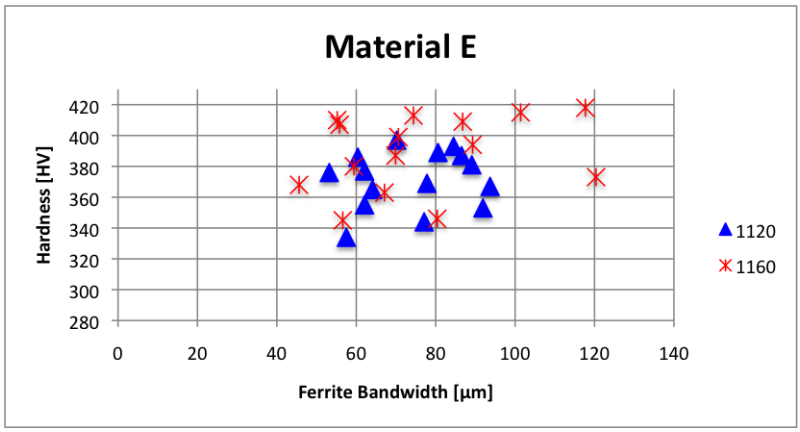

(a) *Microhardness of ferrite in sample E.*

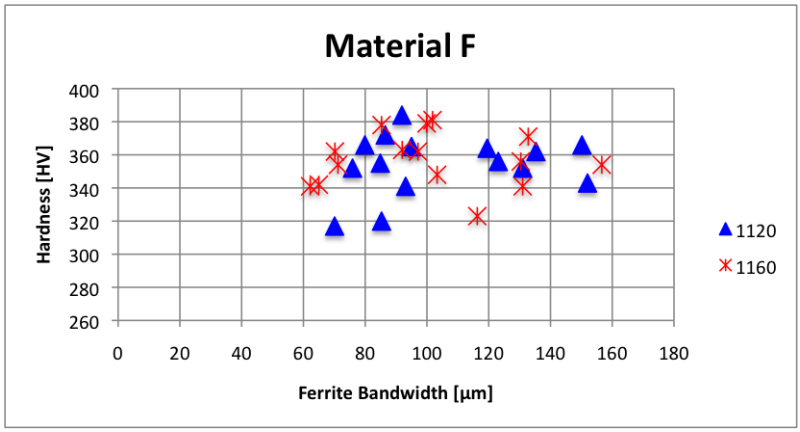

(b) *Microhardness of ferrite in sample F.*

Figure 28: *Microhardness as a function of ferrite bandwidth in samples heat treated at 1120° C and 1160° C.15 indentations were taken in each sample for the two different heat treatment temperatures.*

5.4 Hardness profiles

In the micrographs of the samples heat treated at 1120°C and 1160°C (Fig.16a to 17d) a narrow zone without precipitates is observed along the phase boundary while the highest amount of precipitation appears to take place in the center of the ferrite bands. To study this observation more closely a hardness profile was created by taking microhardness indentations across ferrite bands using a load of 25gf. The results are shown in Fig.29a to Fig.33f with micrographs showing the placement of the indentations. The samples heat treated at 1120°C and 1160°C show an increased hardness towards the center of the ferrite band consistent with an increased amount of precipitation. In the samples heat treated at 1060°C, with little or no sign of precipitation, a small variation of hardness is observed throughout the ferrite band but no indications of the center being the hardest section.

5.5 Charpy tests

Charpy test was performed on specimens from a UNS S32760 superduplex component. The microstructure of the material as received was studied and is shown in the micrograph in Fig.34. The austenite spacing of the material was calculated and found to be $38{,}5\mu m$, similar to previously studied materials, and the microstructure may be classified as relatively coarse. The microstructure does however differ from the other alloys as a significant amount of intragranular austenite is observed within the thick ferrite regions. Charpy tests were performed on specimens heat treated at 1120°C and 1160°C, along with a set of specimens not heat treated used as reference material. A series of three specimens were used for each heat treatment temperature and the results are presented in Table 11 along with the average values for each series. The microstructure of the heat treated Charpy specimens are shown in Fig.35a and 35b. Intragranular nitrides are not observed in the specimen heat treated at 1120°C, but precipitation is clearly visible in the specimen heat treated at 1160°C. The specimens were imaged after testing and the fractures are shown in Fig.36 to Fig.38. Samples 1-3, heat treated at 1120°C, and samples 7-9, reference samples, all showed a ductile behaviour with high Charpy values of 296 J and rough fracture surfaces with jagged edges and shear lips consistent with a ductile fracture. Samples 4-6, heat treated at 1160°C, showed significantly lower Charpy values and fracture surfaces was observed with smooth areas indicating a less ductile fracture.

5.6 XRD

Diffraction analysis was performed on sample A heat treated at 1160°C as this have shown the most amount of nitride precipitation and thus, if possible to detect, were expected to show the clearest results of the presence of chromium nitrides. The X-ray diffraction results are shown in Fig.39. The peaks correspond to a iron-chromium-nickel material which corresponds to the most important elements in sample A. There is however no peaks indicating the presence of Cr_2N nor other nitrides. Diffraction analysis was therefore not successful in detecting and verifying the presence of intragranular nitrides. This may be due to their small size and little fraction compared to the other phases of the material. Other methods should be applied to verify their presence such as the use of transmission electron microscopy where Cr_2N have been successfully characterized previously.

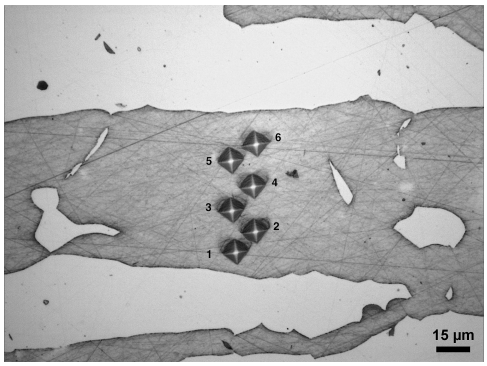

(a) *Hardness indentations across ferrite band of 73µm. Sample 1 heat treated at 1060° C.*

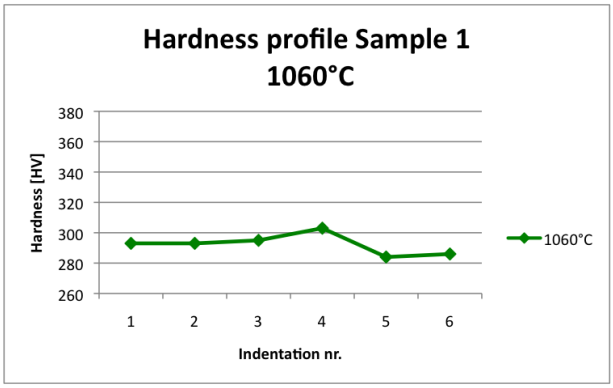

(b) *Hardness profile across ferrite band. Sample 1 heat treated at 1060° C.*

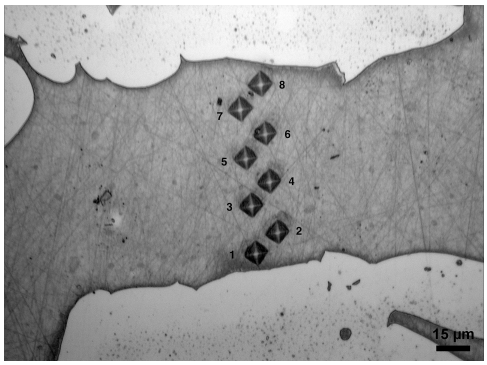

(c) *Hardness indentations across ferrite band of 92µm. Sample 1 heat treated at 1120° C.*

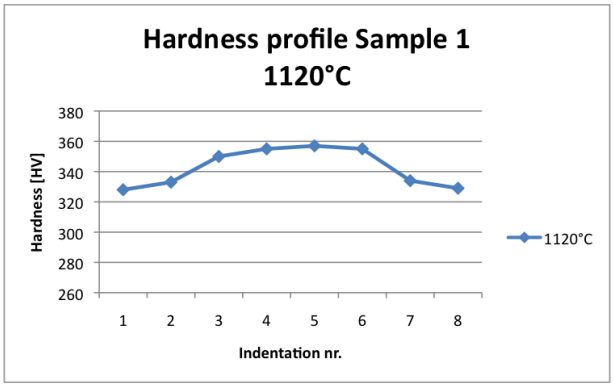

(d) *Hardness profile across ferrite band. Sample 1 heat treated at 1120° C.*

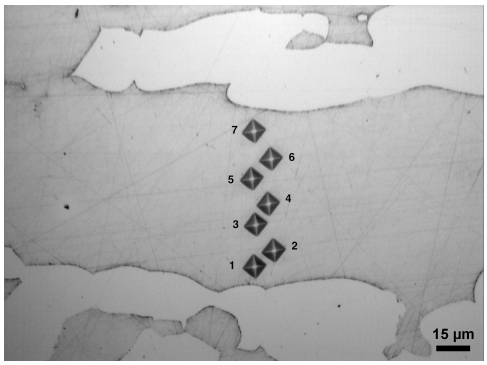

(e) *Hardness indentations across ferrite band of 79µm. Sample 1 heat treated at 1160° C.*

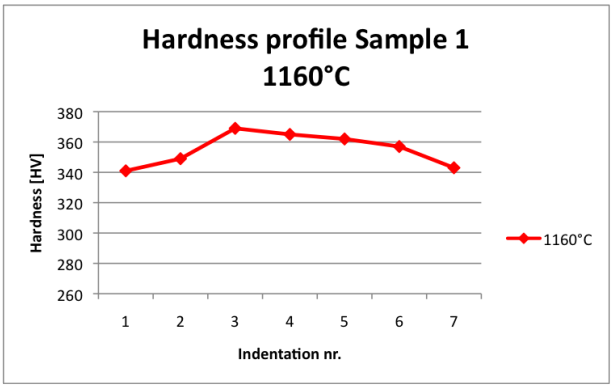

(f) *Hardness profile across ferrite band. Sample 1 heat treated at 1160° C.*

Figure 29: *Microhardness profile of alloy 1.*

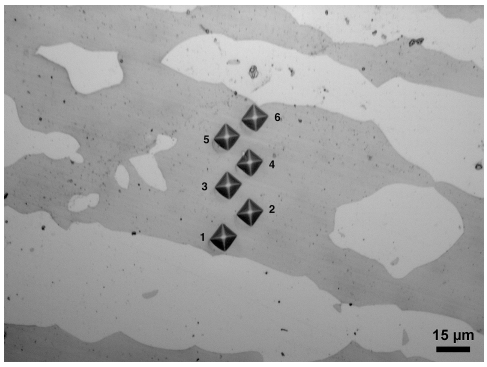

(a) *Hardness indentations across ferrite band of 69µm. Sample 4 heat treated at 1060° C.*

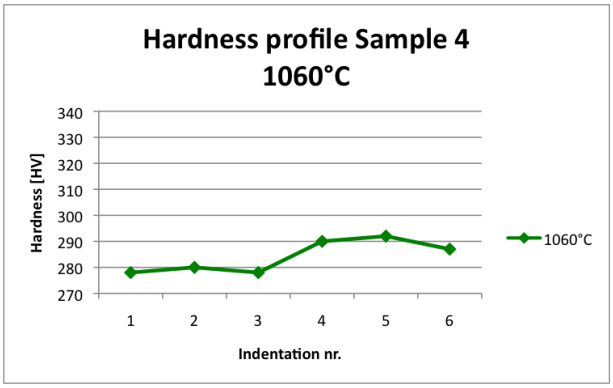

(b) *Hardness profile across ferrite band. Sample 4 heat treated at 1060° C.*

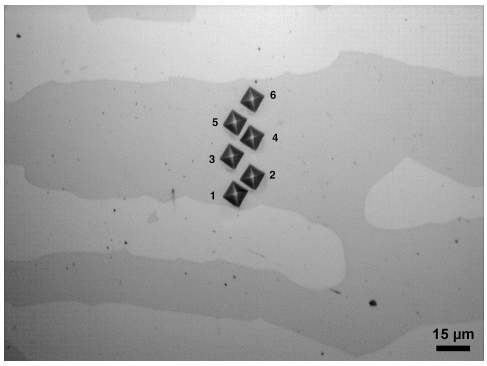

(c) *Hardness indentations across ferrite band of 58µm. Sample 4 heat treated at 1120° C.*

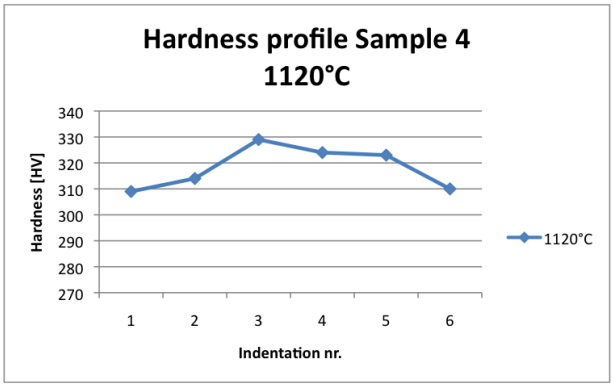

(d) *Hardness profile across ferrite band. Sample 4 heat treated at 1120° C.*

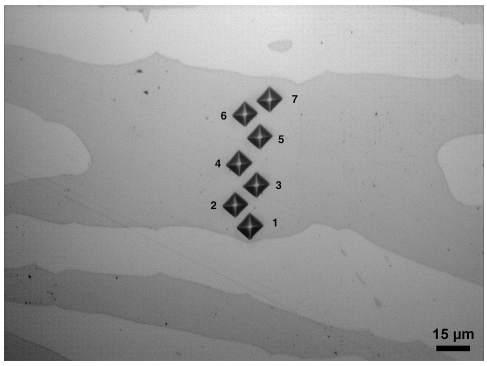

(e) *Hardness indentations across ferrite band of 74µm. Sample 4 heat treated at 1160° C.*

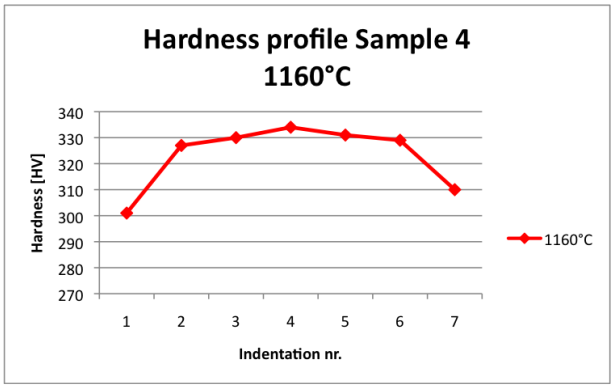

(f) *Hardness profile across ferrite band. Sample 4 heat treated at 1160° C.*

Figure 30: *Microhardness profile of alloy 4.*

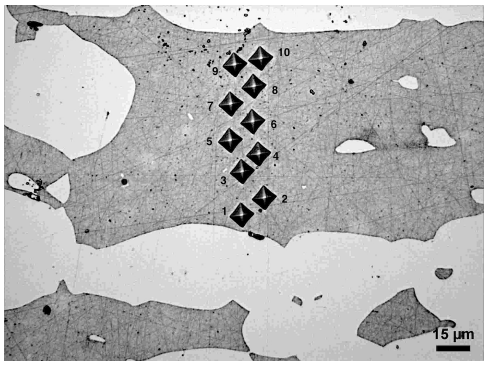

(a) *Hardness indentations across ferrite band of 89µm. Sample A heat treated at 1060° C.*

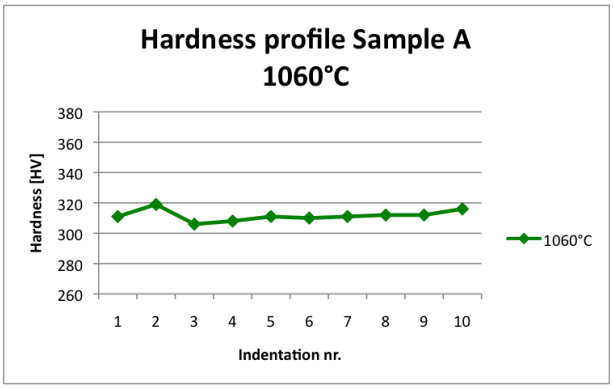

(b) *Hardness profile across ferrite band. Sample A heat treated at 1060° C.*

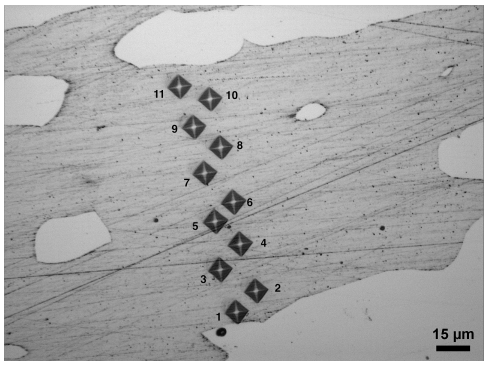

(c) *Hardness indentations across ferrite band of 115µm. Sample A heat treated at 1120° C.*

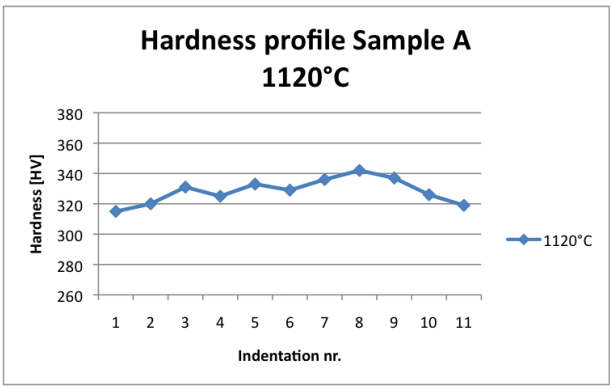

(d) *Hardness profile across ferrite band. Sample A heat treated at 1120° C.*

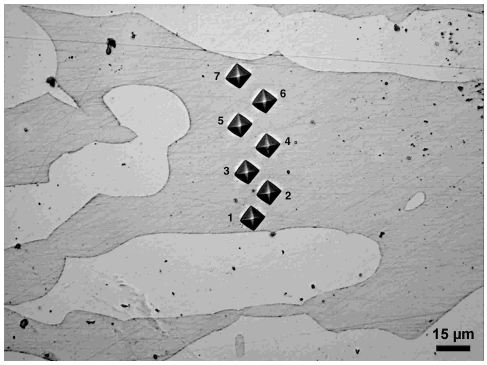

(e) *Hardness indentations across ferrite band of 76µm. Sample A heat treated at 1160° C.*

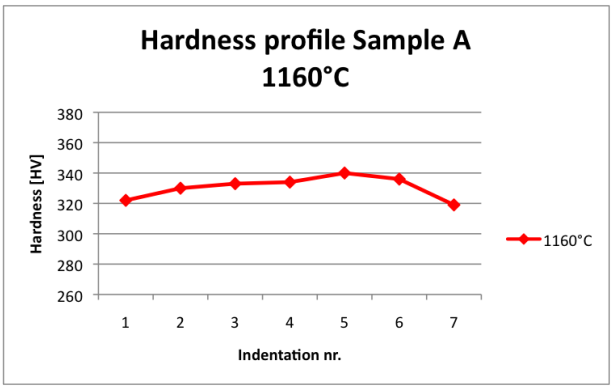

(f) *Hardness profile across ferrite band. Sample A heat treated at 1160° C.*

Figure 31: *Microhardness profile of alloy A.*

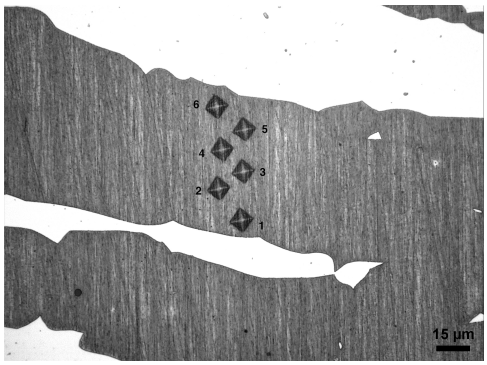

(a) *Hardness indentations across ferrite band of 65µm. Sample C heat treated at 1060° C.*

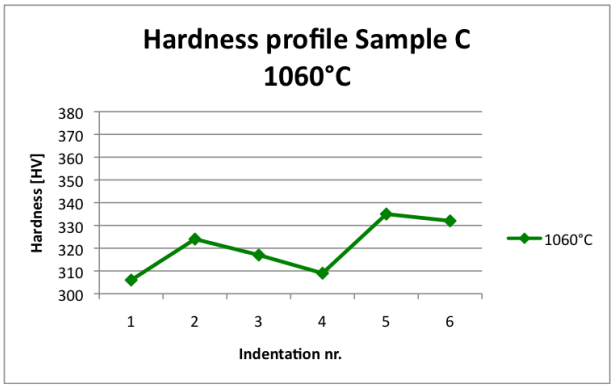

(b) *Hardness profile across ferrite band. Sample C heat treated at 1060° C.*

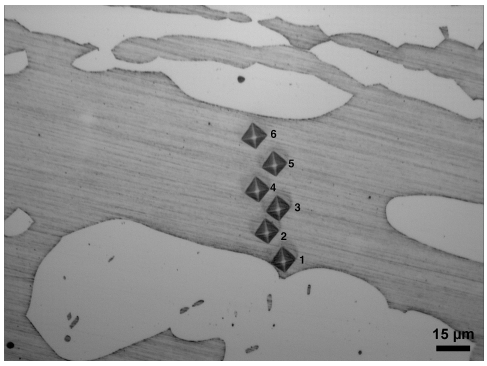

(c) *Hardness indentations across ferrite band of 69µm. Sample C heat treated at 1120° C.*

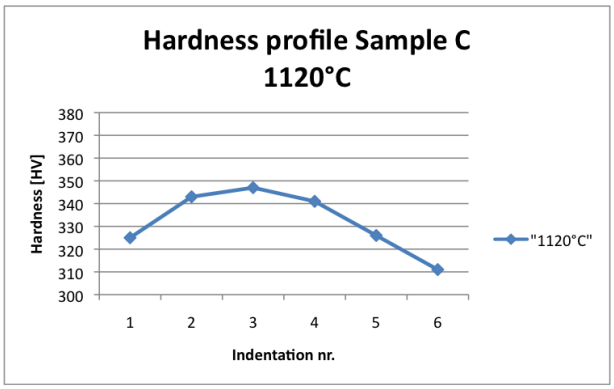

(d) *Hardness profile across ferrite band. Sample C heat treated at 1120° C.*

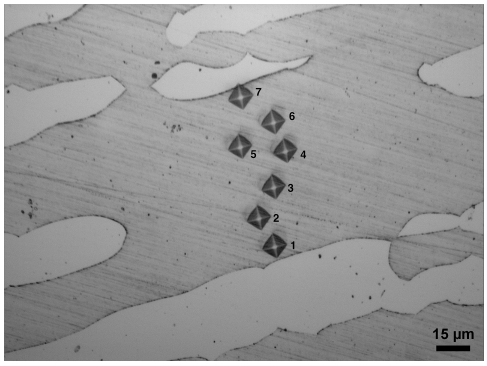

(e) *Hardness indentations across ferrite band of 79µm. Sample C heat treated at 1160° C.*

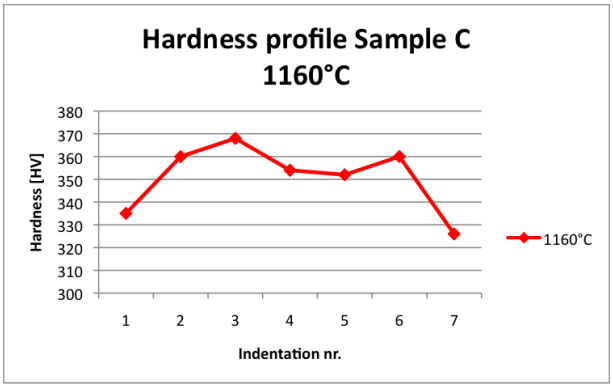

(f) *Hardness profile across ferrite band. Sample C heat treated at 1160° C.*

Figure 32: *Microhardness profile of alloy C.*

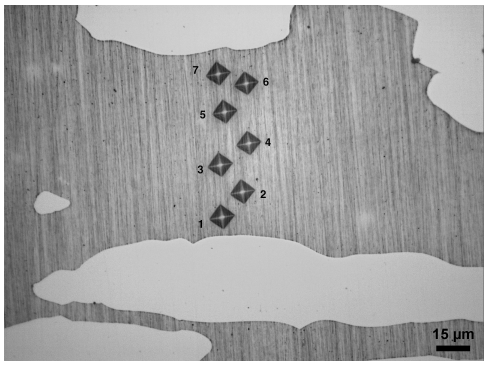

(a) *Hardness indentations across ferrite band of 83µm. Sample F heat treated at 1060° C.*

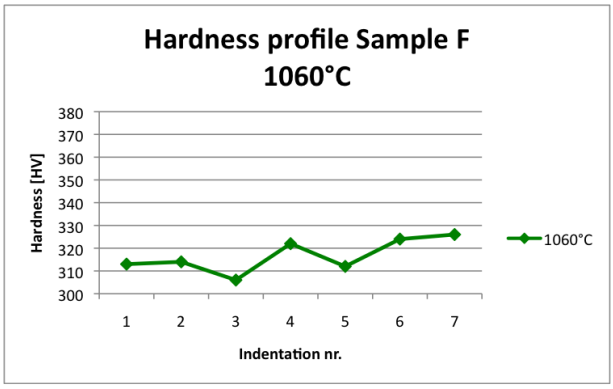

(b) *Hardness profile across ferrite band. Sample F heat treated at 1060° C.*

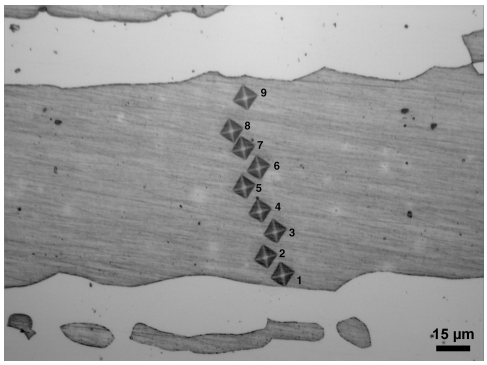

(c) *Hardness indentations across ferrite band of 92µm. Sample F heat treated at 1120° C.*

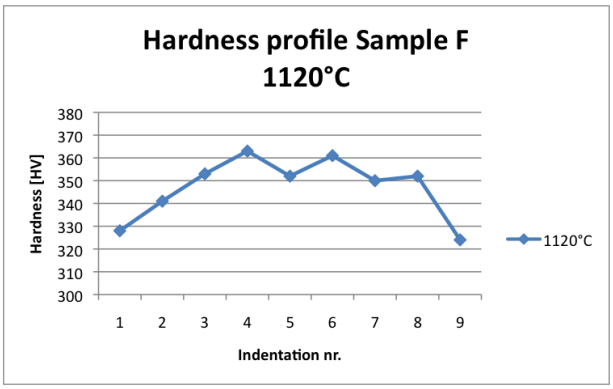

(d) *Hardness profile across ferrite band. Sample F heat treated at 1120° C.*

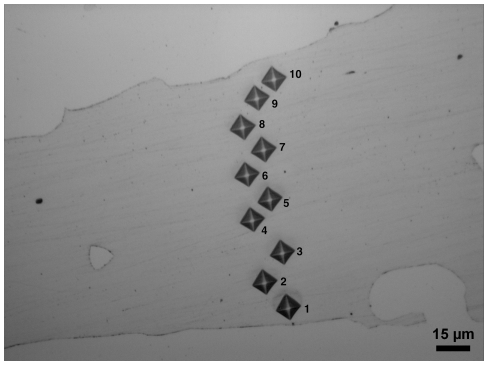

(e) *Hardness indentations across ferrite band of 114µm. Sample F heat treated at 1160° C.*

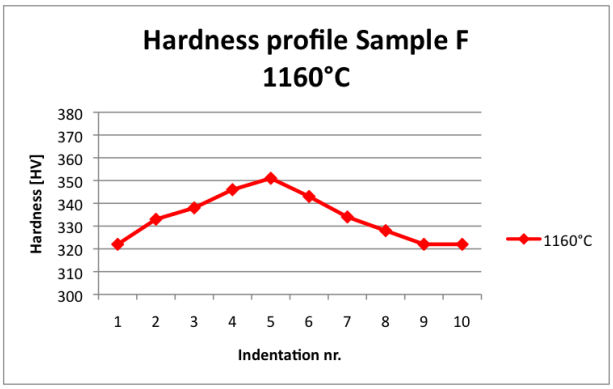

(f) *Hardness profile across ferrite band. Sample F heat treated at 1160° C.*

Figure 33: *Microhardness profile of alloy F.*

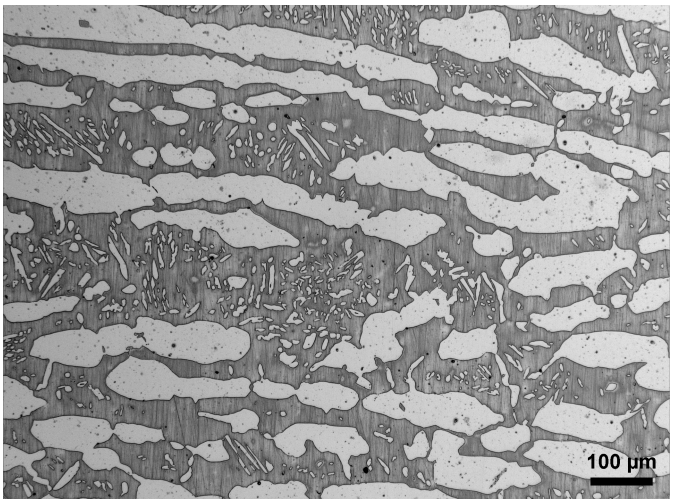

Figure 34: *Micrograph of Charpy material in the as received condition. Note the large amounts of secondary austenite within ferrite regions.*

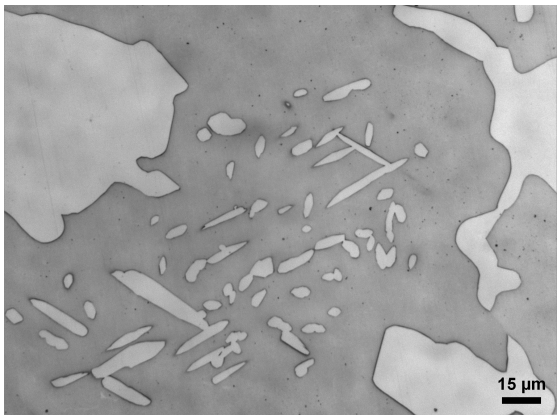

(a) *Micrograph of Charpy specimen 1 heat treated at 1120° C. No nitride precipitation observed.*

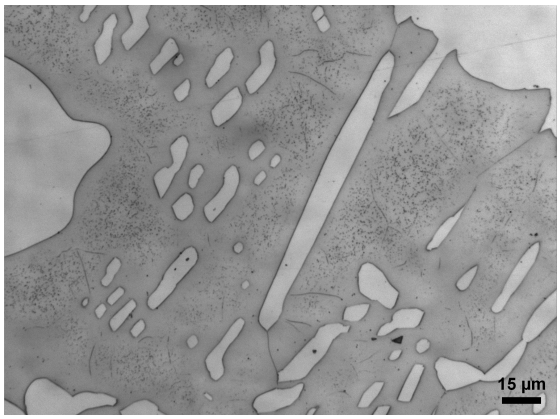

(b) *Micrograph of Charpy specimen 4 heat treated at 1160° C. Nitride precipitation observed in the ferrite as well as intragranular austenite.*

Figure 35: *Micrograph of heat treated Charpy specimens.*

Table 11: *Low temperature Charpy V-notch impact test results. Test temperature: -46° C.*

Heat Treatment	Specimen nr.	Charpy values [J]	Average [J]
1120°C	1	296	297
	2	296	
	3	298	
1160°C	4	192	214
	5	280	
	6	170	
As received	7	295	296
	8	296	
	9	296	

Figure 36: *Charpy specimens 1-3 from the right. Heat treated at 1120° C. Specimens showed an average Charpy toughness value of 297 J and ductile fractures with rough fracture surfaces and lateral expansion on both sides of the specimens.*

Figure 37: *Charpy specimens 4-6 from the right with Charpy values of 192, 280 and 170 J respectively. Heat treated at 1160° C. Specimens showed an average Charpy toughness value of 214 J and less ductile fractures than the other specimens.*

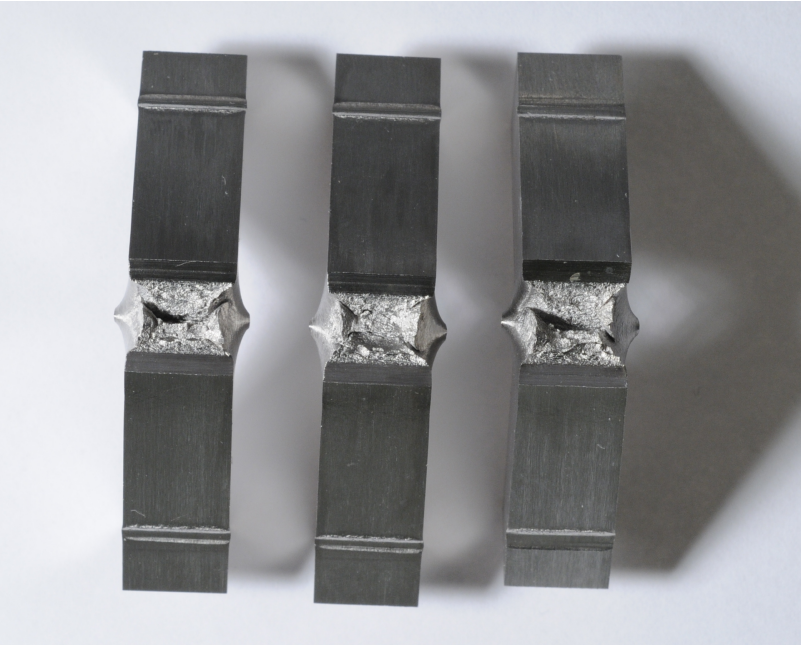

Figure 38: *Charpy specimens 7-9 from the right. Reference material, not heat treated. Specimens showed an average Charpy toughness value of 296 J and ductile fractures with rough fracture surfaces and lateral expansion on both sides of the specimens.*

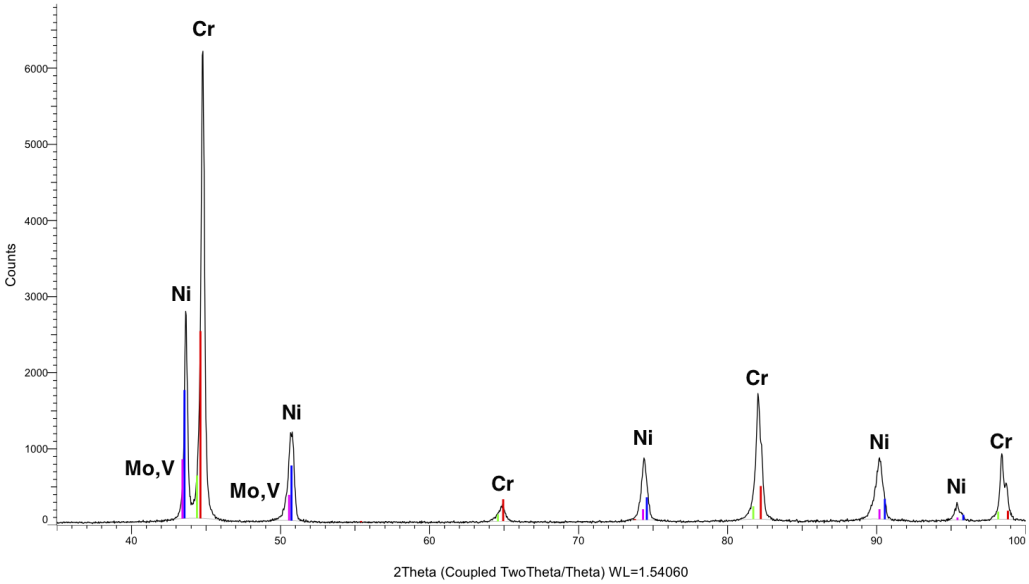

Figure 39: *Xrd diffraction analysis of Material A. Peaks correspond to the alloying elements in the sample. Intragranular nitrides were not detected with this method.*

6 Discussion

6.1 Heat treatment

Four superduplex and duplex alloys were investigated with regards to heat treatment temperature, microstructure and nitrogen content, and the effect of these parameters on the materials susceptibility to intragranular chromium nitride precipitation. Heat treatment temperature is observed to have a great effect on intragranular precipitation, as a clear trend can be seen with increased precipitation at higher heat treatment temperature. This may be observed both in the micrographs showing the microstructure of the samples (Fig.15a to 17d) and in the graphs with the quantified amount of nitrides (Fig.18a to 19b). All the alloys display the similar trend, with the duplex alloy containing the lowest fraction of precipitates of the samples investigated. Almost no precipitation is observed in the samples heat treated at 1060°C, the temperature is therefore sufficiently high to dissolve the nitrides observed in the samples in the as received condition while avoiding new precipitates forming during cooling. Increasing the heat treatment temperature to 1120°C and 1160°C results in severe and intense precipitation. This difference is related to the rapid drop in solubility of nitrogen in ferrite at 1050 - 1100°C observed in Fig.3. A heat treatment temperature of 1060°C is sufficiently low to keep most of the nitrogen in the austenite and result in less diffusion into ferrite than at higher temperatures where the solubility of ferrite increases and the difference in solubility between the two phases decreases. The result is less nitrogen trapped in the ferrite during rapid cooling and thus less nitride precipitation. Low heat treatment temperatures are therefore beneficial to avoid nitride precipitation. However, intermetallic precipitates are more detrimental than nitrides and the heat treatment temperature must be kept sufficiently high as to avoid entering the stability area of intermetallic phases in the TTT diagram (Fig.2).

Quantifying the nitride precipitation and plotting it as a function of ferrite bandwidth revealed a clear trend towards higher degree of precipitation with an increased austenite spacing. Broader ferrite bands involve an increased diffusion distance for nitrogen. During rapid cooling this increased diffusion distance prevents the nitrogen from diffusing into the austenite, resulting in more precipitation of nitrides. Only in microstructures with very small austenite spacing or in a narrow zone close to the phase boundaries in broader ferrite bands will the nitrogen have sufficient time to diffuse from the ferrite, creating a zone without precipitation. Grain boundaries and subcell boundaries affects the amount of precipitation. Nitrides form on both types of boundaries, but only along grain boundaries does a precipitate free zone appear. Cellular substructures exhibit a high boundary-dislocation density and very small cell disorientation angles [23]. The disorientation angles may affect the precipitation and cause the different precipitation behaviour and further studies should be done regarding this phenomenon. An increase in austenitic phase at the expense of ferrite is beneficial in regards of nitride precipitation as austenite dissolves much more nitrogen and exhibits no problems with this phenomenon. The phase balance is however crucial to the mechanical properties and a significant shift in the phase balance may have a negative effect on the mechanical properties of the component.

The materials studied were alloys within three different UNS standards. Three superduplex alloys with relatively similar composition and a 22Cr duplex alloy. The most important factor of the chemical composition with regards to the materials susceptibility to nitride precipitation is believed to be the nitrogen content. Comparing the amount of

nitride precipitation in the specimens revealed overlapping results (Fig.20a and Fig.20b). This was to be expected as the superduplex alloys showed a very small variation in nitrogen content. Compared to previously studied samples there is a indication towards higher fraction of precipitates with higher nitrogen content, specially at broader ferrite bands and at higher heat treatment temperatures. The duplex alloy containing the least amount of nitrogen show a overall lower fraction of precipitates while material A containing the highest amount of nitrogen reveal the highest fraction of precipitates. The differences in nitride fractions caused by varying nitrogen content is however much smaller than the differences caused by temperature and microstructure. Nitrogen is added intentionally and is an important alloying element in providing the phase balance between ferrite and austenite. A high nitrogen content is not ideal with regards to nitride precipitation but it facilitates the formation of austenite that in turn accommodates the majority of the nitrogen, reducing the materials susceptibility to nitride formation. The nitrogen content thus has a much smaller effect on nitride precipitation than microstructure and heat treatment temperature.

The results obtained in the heat treatment experiments confirm the observations made in the previous project with a low heat treatment temperature and short austenite spacing being the most influential and beneficial factors in order to minimize the precipitation of intragranular chromium nitrides. A combination of high nitrogen content, coarse microstructure and rapid cooling after exposure to high temperatures are all factors that increases the materials susceptibility to nitride precipitation.

6.2 Microhardness

Initial investigations performed by Statoil indicated that intragranular chromium nitrides affects the hardness of the ferritic phase. Microhardness tests was therefore performed with indentations located in the ferrite and austenite phases separately. Microhardness testing of in all 10 alloys revealed a clear trend of increasing hardness of the ferrite with increased heat treatment temperature (Fig.21a to Fig.24b). The hardness of the austenite remained virtually unaffected regardless of heat treatment temperature, which was to be expected considering nitride precipitation only occurs in ferrite and the austenite does not experience any second phase precipitation. The high alloying content of substitutional elements causes solid solution hardening of both phases and as expected, the duplex alloy containing the least amount of alloying elements showed the overall lowest hardness values. Interstitially dissolved nitrogen increase the microhardness of austenite as it can dissolve a much higher amount of nitrogen than ferrite and the addition of nitrogen causes solid solution hardening. This hardening effect does not change substantially in the heat treatment temperature range used in this experiment, and the hardness of the austenitic phase is left fairly constant. Ferrite has a very low solubility limit of nitrogen and in addition to solid solution hardening from substitutional elements it becomes supersaturated on nitrogen and experiences particle hardening from the precipitation of chromium nitrides. The particle hardening effect depends on the amount of nitrides, thus the ferrite becomes harder at higher heat treatment temperatures when the amount of precipitates increases.

The alloy showing the highest hardness values was sample E. The nitrogen content of this alloy (0,221%) is relatively low, but this alloy has the highest forging ratio resulting in the lowest austenite spacing of the alloys tested. Processing and the resulting microstructure

thus is an important factor regarding the initial hardness of the material. The duplex alloy with lowest hardness, contained the least amount of nitrogen and the lowest fraction of precipitates. The hardening effect experienced at temperatures resulting in nitride precipitation is however approximately the same as the higher alloyed superduplex alloys. The presence of nitrides thus give a significant hardening effect even at lower amounts of precipitates. The initial hardening effect appear more prominent than the hardening due to the actual amount of nitrides, indicated with the relatively low differences in hardness between samples heat treated at 1120°C and 1160°C for several of the alloys. The indentations are taken approximately in the center of the ferrite bands where the precipitation is believed to be at its most severe, but as the indentations are taken on samples not etched with oxalic acid, the precipitations are not visible upon microhardness testing. The deviations in hardness values are relatively large. This may be caused by inhomogeneous distribution of chromium nitrides in the ferrite and the fact that the indentations are taken in ferrite bands of varying width, from approximately 40μm to 160μm, which results in a varying fraction of precipitates in the ferrite bands. Any evaluation of results from a microhardness test should be done with the knowledge that the scattering of results obtained in the test is quite large given that the maximum microhardness values obtained in the ferrite does not lie within the standard deviation range. An exact figure of how much nitride precipitation will affect the microhardness of the material is not possible to obtain, but a significant hardening will occur and several extremely hard individual values must be expected.

The quantification of nitride fractions revealed precipitation in ferrite bands as thin as $20\mu m$. Microhardness indentations were not taken in such thin ferrite bands as the size of the indentation marks using a load of 200gf would exceed the size of the ferrite region. Indentations affected by a phase boundary and the surrounding austenite would not give a correct evaluation of the microhardness of the ferrite and for this reason, only ferrite regions wider than $40\mu m$ were investigated. It has previously been shown that the amount of nitride precipitation depends strongly on the microstructure of the samples. The microhardness of the ferrite was expected to increase with increasing ferrite bandwidth, as the amount of precipitates increases in samples heat treated at 1120°C and 1160°C. The results shown in Fig.25a to Fig.28b show this overall correlation in the samples, although some exceptions are observed where broad ferrite bands display low hardness values and thin ferrite bands display surprisingly high hardness values. The indentations were placed approximately in the center of each ferrite region, where precipitation was believed to be most severe, but inhomogeneous precipitation and subgrain boundaries may have affected the results. The hardness values are thus not independent of indentation placement within the ferrite.

6.3 Hardness profile

In the micrographs of the heat treated samples showing nitride precipitation (Fig.16a to Fig.17d) a narrow precipitation free zone close to the phase boundaries was observed in the ferrite. The amount of precipitation appears to increase towards the center of the ferritic region. In order to examine this observation more closely a hardness profile was created by taking microhardness indentations across ferrite bands in five of the alloys. The results show an increased hardness in the center of the ferrite bands for the samples heat treated

at 1120°C and 1160°C (Fig.29a to Fig.33f). The hardening of the center correlates to the intense precipitation observed in the samples heat treated at these temperatures and corresponding precipitation hardening. The observations and hardness values show that diffusion distance greatly affects the precipitation and consequently the microhardness of ferrite. Nitrogen can only diffuse short distances during rapid cooling, leaving a narrow precipitation free zone along the phase boundaries where the nitrogen has had sufficient time to reach the surrounding austenite. This zone consequently show the lowest hardness values as no precipitation hardening takes place. The precipitation increases with increased diffusion distance towards the center where more nitrogen remains trapped in the ferritic region. The samples heat treated at 1060°C showed no or little signs of nitride precipitation after heat treatment (Fig.15a to 15d). The hardness profile of these samples showed some variation in hardness across the ferrite bands, but the areas closest to the phase boundaries did not reveal systematically lower hardness values nor was there an indication of the center being the hardest part of the ferrite region. The variation in microhardness may come from other microstructure features such as subgrain boundaries which are not visible when performing the microhardness test.

6.4 Charpy tests

Charpy test was performed to investigate the toughness of UNS S32760 superduplex stainless steel after heat treatment at 1120°C and 1160°C. These temperatures have shown to give intense and severe precipitation of intragranular chromium nitrides, and thus believed to be suitable for investigating the nitrides influence on the impact toughness of the material. The specimens used as reference material were not heat treated and showed as expected very good Charpy values of 296 J. The results were also very consistent as the minimum value obtained was 295 J. The fracture surfaces confirm the results as all the specimens show a rough fracture surface (Fig.38) with a lot of topography and jagged edges. The specimens also show lateral expansion to both sides indicating a ductile specimen. The specimens heat treated at 1120°C showed no sign of reduced impact toughness as the results were identical to that of the reference material. The fracture surfaces of the specimens also showed the same ductile behaviour as observed in the non heat treated samples. In the specimens heat treated at 1160°C the Charpy values dropped significantly with an average value of 214 J, a overall reduction of close to 30% from the non heat treated reference material. The lowest obtained value was 170 J, a reduction in Charpy value of over 40%. A reduction was to be expected as this heat treatment temperature will result in severe precipitation of intragranular chromium nitrides in the ferrite, causing embrittlement of the material. Specimen number 5 showed little reduction with a Charpy value of 280 J indicating a ductile material. Compared to the fracture surface of specimens 4 and 6 (Fig.37) with significantly lower Charpy values, fracture surface of specimen 5 show a slight difference with an increased size of the shear lips and a rougher topology, indicating a higher charpy toughness value. The least ductile specimens both show a smoother fracture surface than the other specimens, confirming the values obtained in the tests. The series of specimens heat treated at 1160°C was the only series with a wide variation of Charpy values, with results ranging from 170 to 280 J. This variation may have been caused by inhomogeneous precipitation of chromium nitrides in the microstructure, leading to a varying degree of embrittlement within the material. The results are therefore sensitive to the location from which the specimens are cut and the location of

the notch.

The specimens heat treated at 1120°were expected to show a decreased impact toughness as a significant amount of chromium nitrides have shown to precipitate after heat treatment at this temperature. The results does however show no indications of embrittlement of the material. The reason for the unexpected results lay in the microstructure of the material used for the Charpy test as no nitride precipitation is observed in the specimens heat treated at 1120°C. The austenite spacing is 38,5μm, one of the lowest of the alloys investigated in this project, but still a rather coarse microstructure which should render the material susceptible to nitride precipitation. The great difference in microstructure compared to the other alloys lies in the amount of secondary austenite observed within the large ferrite regions (Fig.34). This intragranular austenite shortens the diffusion distance for nitrogen considerably, making it a lot easier for nitrogen to reach the austenite phase where the solubility of nitrogen is much higher than in ferrite. This will lead to less nitrogen trapped in the ferrite upon rapid cooling, resulting in less nitride precipitation. The material is therefore in general less susceptible to precipitation of intragranular nitrides. Intragranular nitrides are observed in the specimen heat treated at 1160°C (Fig.35b) alongside intragranular secondary austenite. The amount of nitrogen trapped in the ferrite upon rapid cooling was thus so large that the presence of intragranular austenite was not sufficient to prevent nitride precipitation. This correlates well with the reduced Charpy toughness values obtained for these specimens and show the embrittling effect the nitrides have on the material.

The presence of secondary austenite improves the toughness of the material. Charpy tests performed on a material with a microstructure without intragranular austenite would therefore most likely result in a reduction of Charpy values for the series heat treated at 1120°C and even greater reductions in Charpy values for the series heat treated at 1160°C. Production and heat treatment of duplex steels should therefore be chosen to ensure high amounts of austenite and intragranular secondary austenite with regards to improving the toughness of the material. Secondary austenite precipitates upon reheating of duplex steels and a microstructure initially affected by chromium nitrides may be significantly altered by correct heat treatment. The originally brittle microstructure may improve its toughness as chromium nitrides dissolve and act as nucleation sites for secondary austenite.

The Charpy v-notch impact test temperature was -46°C. A standard test temperature according to NORSOK standards. Minimum impact toughness requirements per NORSOK M-630 are for comparison 45 J for average values and 35 J for single specimens, tested at -46°C. All the specimens are thus well above the requirements at this temperature. The drop in impact toughness for specimens heat treated at 1160°C is non the less significant, as superduplex stainless steels are in demand for use in increasingly lower temperatures. Considering that the test was performed on a material not particularly susceptible to nitride precipitation, the detrimental effects on impact toughness could become hazardous at low temperatures and with materials prone to intragranular chromium nitride precipitation.

7 Conclusion

In order to study the phenomenon of intragranular chromium nitride precipitation in duplex and superduplex stainless steels heat treatment experiments, microhardness tests and charpy v-notch impact tests were performed. As there exists no standard method to quantify the amount of chromium nitrides a experimental method tested in a previous project was used in these experiments. The quantification was done by the use of a computer software program which separates the etch pits in ferrite from the ferrite matrix based on the difference in contrast. This result is used as an indirect measure of nitride precipitation and the results presented as the area fraction of nitrides. The experiments have led to the following conclusions:

- The heat treatment experiments confirm what has previously been observed when studying the parameters heat treatment temperature, microstructure and nitrogen content. An increased heat treatment temperature increases the amount of nitride precipitation and should therefore be kept as low as possible, without risking precipitation of intermetallic phases. The fraction of nitrides also increases with an increased ferrite bandwidth. A microstructure with short austenite spacing is beneficial as the diffusion distance for nitrogen becomes smaller, leaving less nitrogen trapped in the ferrite upon rapid cooling. The nitrogen content does not affect the amount of precipitation to the same extent as the heat treatment temperature and microstructure. However, a high nitrogen content in combination with coarse microstructure and too high heat treatment temperature will increase the materials susceptibility to intragranular chromium nitride precipitation.
- The nitride precipitation affects the microhardness of the ferrite by causing particle hardening, and the microhardness of the phase increases with heat treatment temperature and amount of precipitation. The microhardness of the austenite is left unaffected by this phenomenon as no particle hardening takes place in this phase.
- The microhardness of the ferrite increases towards the center of the ferrite regions, where precipitation is at its most severe. A narrow precipitation free zone appears along the phase boundaries where nitrogen has had time to diffuse into the austenite, resulting in lower microhardness values than in the center of the region where diffusion distance is much longer.
- Charpy impact test reveal the embrittling effect intragranular chromium nitrides have on the impact toughness of superduplex steel. However, the toughness improves with a high amount of intragranular secondary austenite in the microstructure. The intragranular austenite shortens the diffusion distance of nitrogen resulting in less nitrogen trapped in the ferrite and leaving the material less susceptible to nitride precipitation.

Acknowledgements

I wish to thank my supervisor Jan Ketil Solberg who has contributed with valuable discussions and ideas regarding both execution and results of the thesis. The contributions of co-supervisor Mads Aursand is gratefully acknowledged. He was of great help with performing the Charpy tests and his knowledge and background material on the subject were essential for the thesis. The support of Statoil providing the materials used and the equipment used in the charpy tests is also greatly acknowledged. Furthermore I wish to thank Julian Tolchard and Astri Sømme for introduction and help in the XRD laboratory.

References

[1] Mads Aursand, Gisle Rørvik, and Knut Sjølstad; Statoil ASA Trondheim. Chromium nitride precipitates in large super duplex stainless steel forged components. Draft from upcoming Statoil presentation.

[2] J.-O. Nilsson. Super duplex stainless steels. *Materials Science and Technology*, 8:685–700, August 1992.

[3] B.I.Voronenko. Austenitic - ferritic stainless steels: A state of the art review. *Metal Science and Heat Treatment*, 39:428–437, 1997.

[4] Henrik Sieurin. *Fracture toughness properties of duplex stainless steels.* PhD thesis, Royal Institute of Technology, Stockholm, Sweden, 2006, pp:7 - 27.

[5] Carpenter Stainless Steel "Blue Book", Welding of Stainless Steels, accessed 23.01.2012 http://www.cartech.com/techarticles.aspx?id=1830.

[6] T.H.Chen, K.L. Weng, and J.R. Yang. The effect of high-temperature exposure on the microstructural stability and toughness property in a 2205 duplex stainless steel. *Materials Science and Engineering A338*, pages 259–270, 2002.

[7] John C. Lippold and Damian J. Kotecki. *Welding Metallurgy and Weldability of Stainless Steels.* John Wiley & Sons Inc., 2005. Chapter 7, pp.230-261.

[8] H.Hänninen, J.Romu, R.Ilola, J.Tervo, and A.Laitinen. Effects of processing and manufacturing of high nitrogen-containing stainless steels on their mechanical, corrosion and wear properties. *Journal of Material Processing Technology*, 117:424–430, 2001.

[9] J.D. Kordatos, G. Fourlaris, and G. Papadimitriou. The effect of cooling rate on the mechanical and corrosion properties of SAF 2205 (UNS 31803) duplex stainless steel welds. *Scripta materialia*, (44):401–408, 2001.

[10] J.-O. Nilsson and G. Chai. The physical metallurgy of duplex stainless steels. Sandvik Materials Technology, R&D Centre,Sweden, 2010. Duplex World 2010, Beune, France.

[11] W.Horvath, W.Prantl, H Stroissnigg, and E.A.Werner. Microhardness and microstructure of austenite and ferrite in nitrogen alloyed duplex steels between 20 and 500°C. *Materials Science and Engineering A256*, pages 227–236, 1998.

[12] W.Horvath, B.Tabernig, E.Werner, and P.Uggowitzer. Microstructures and yield strength of nitrogen alloyed super duplex steels. *Acta Materialia*, 45(4):1645–1654, 1997.

[13] T.H.Chen and J.R. Yang. Microstructural characterization of simulated heat affected zone in a nitrogen-containing 2205 duplex stainless steel. *Materials Science and Engineering A338*, pages 166–181, 2002.

[14] Carlos Mario Garzón, Carlos A.Serna, Sérgio D.Brandi, and Antonio J.Ramirez. The relationship between atomic partitioning and corrosion resistance in the weld-heat affected zone microstructures of UNS S32304 duplex stainless steel. *Journal of Material Science*, 42:9021–9029, 2007.

[15] Zhang Wei, Jiang Laizhu, Hu Jincheng, and Song Hongmei. Effect of ageing on precipitation and impact energy of 2101 economical duplex stainless steel. *Materials Characterization*, 60:50–55, 2009.

[16] A.J. Ramirez, J.C. Lippold, and S.D. Brandi. The relationship between chromium nitride and secondary austenite precipitation in duplex stainless steels. *Metallurgical and Materials Transactions*, 34A:1575–1597, 2003.

[17] J.O.Nilsson and A.Wilson. Influence of isothermal phase transformations on toughness and pitting corrosion of super duplex stainless steel SAF 2507. *Materials Science and Technology*, 9:545–554, 1993.

[18] R. Francis G.Byrne and G. Warburton. Variation in mechanical properties and corrosion resistance of different alloys within the generic designation UNS S32760. Originally presented at DUPLEX 2000, Houston,TX,USA,Feb.2000.

[19] *ASM Handbook - Metallography and Microstructures*, volume 9. ASM International, 2004. pp.670-675.

[20] Det Norske Veritas. *DNV RP-F112, Design of Duplex stainless steel subsea equipment exposed to cathodic protection*, October 2008.

[21] ASTM International. *E384 - 11. Standard Test Method for Knoop and Vickers Hardness of Materials.*

[22] TWI Ltd United Kingdom, FAQ: What is Charpy Testing?, accessed 07.06.2012 http://www.twi.co.uk/services/technical-information/faqs/material-faqs/faq-what-is-charpy-testing/.

[23] L. I. Tushinskii and A. A. Bataev. Substructural hardening of steel. *Russian Physics Journal*, 34(3):237–243, 1991.

Appendix A – Results from quantification of nitride fraction

The numbers for area fraction of nitrides obtained by the software Image Access Easy Lab are listed in the tables below for the various specimens and heat treatment temperatures.

Table 12: *Results of area phase fraction studies of material 1 heat treated at 1120° C*

Location	Ferrite bandwidth [μm]	Inspected Area [μm^2]	Area fraction [%]
1	40,4	400,9	2,9
2	57,7	501,8	6,7
3	30,3	201,9	2,9
4	54,6	747,6	6,5
5	24,1	148,2	1,4
6	35,2	242,3	3,1
7	46,8	432,5	2,6
8	33,3	117,1	2,5
9	37,8	233,6	3,2
10	69,1	1068,7	7
11	43,7	593,3	4,5
12	44,6	428,2	4,9
13	52,8	441,1	4,8
14	53,2	508,7	5,5
15	34,3	220,9	2,4
16	31,7	205,5	3,4
17	41,5	305,2	3,6
18	52,1	439,1	5,6
19	27,6	172,4	2,4
20	45,8	309,5	4,9

Table 13: *Results of area phase fraction studies of material 1 heat treated at 1160° C*

Location	Ferrite bandwidth [μm]	Inspected Area [μm^2]	Area fraction [%]
1	29,8	223	4,5
2	41,9	575,3	7,4
3	27	399,1	4,7
4	48,9	647,9	7,4
5	45,8	487,9	6,6
6	38,3	532,9	6,4
7	69,4	1465	8,3
8	51,9	829,3	8
9	21,3	110,4	1,7
10	30,4	159	3,5
11	62,7	634,4	8,2
12	46,1	592,8	6
13	22,7	128,9	1,5
14	57,3	523,8	6,9
15	52,1	721	7,3
16	46,4	584,5	6,5
17	32,7	401,7	5,2
18	59,2	773,7	7,5
19	28,2	167,1	3,6
20	66,4	1250	8,5

Table 14: *Results of area phase fraction studies of material 2 heat treated at 1120° C*

Location	Ferrite bandwidth [μm]	Inspected Area [μm^2]	Area fraction [%]
1	48,2	404,7	3,2
2	42,2	330,5	2,5
3	49,4	586,3	4,2
4	45,7	626,7	3,4
5	50,6	358,9	4
6	37,8	234	3
7	65	688,5	5,2
8	28,9	191,6	1,2
9	41,5	356,8	3
10	30,6	151,7	2,1
11	47,8	386,1	2,8
12	36,7	355,8	2,4
13	55,5	546,1	4,6
14	46,3	424,8	2,5
15	40,9	247,6	4,1
16	48,1	451,5	4,5
17	74,2	819,2	5,3
18	65,5	786,9	5,1
19	42,4	565,2	3,3
20	57,4	496,4	4

Table 15: *Results of area phase fraction studies of material 2 heat treated at 1160° C*

Location	Ferrite bandwidth [μm]	Inspected Area [μm^2]	Area fraction [%]
1	41,9	287,2	4,5
2	54	690,7	5,6
3	17,1	89,1	2,1
4	79	1098	8,3
5	35,5	437,3	4,3
6	50,3	641,9	4,7
7	37,5	532,6	5,5
8	66,5	1105,5	7,2
9	60,3	834,4	7,4
10	18,1	164,1	2,6
11	22,5	130,7	2,8
12	36,3	492,3	4,1
13	32,7	204,5	3,8
14	71,3	1090,3	8,1
15	48,2	589,1	6,4
16	30,1	245,8	3,6
17	57,6	636,8	6,5
18	65,4	800,9	7,1
19	49	573,7	5,2
20	23,2	143,4	3,5

Table 16: *Results of area phase fraction studies of material 3 heat treated at 1120° C*

Location	Ferrite bandwidth [μm]	Inspected Area [μm^2]	Area fraction [%]
1	65,7	852,9	6,1
2	43,4	423,6	3,8
3	48,6	584,1	4,2
4	55,5	560,6	5
5	30,1	143,1	1,7
6	49,2	766,7	5,2
7	46,8	586,8	3,1
8	40,5	452,1	3,2
9	37,8	484,6	3
10	32,3	182,5	1,9
11	25	259,9	1,3
12	37,2	346,3	3,6
13	68,2	968,8	5,2
14	26,1	201,1	1,1
15	27,7	211,9	2,8
16	33,2	190,1	2,7
17	39,8	287,8	3,5
18	64,8	691,4	5,8
19	31,8	293,3	2,6
20	44,2	443,5	3,4

Table 17: *Results of area phase fraction studies of material 3 heat treated at 1160° C*

Location	Ferrite bandwidth [μm]	Inspected Area [μm^2]	Area fraction [%]
1	29,6	380,8	6,3
2	40,9	424,8	6,9
3	31,5	314,4	5,3
4	15,8	103,7	1,8
5	51,3	1117,7	6,8
6	28,8	358,4	4,5
7	32,5	366,9	6,3
8	33,7	344,5	5,2
9	55,6	724,9	5,8
10	30	241,1	4
11	41,3	596,8	6,6
12	45,4	340,9	7,2
13	25,7	157,2	4,3
14	35,7	293,9	5,8
15	65,3	1084,8	7,5
16	44,7	467,4	5,8
17	22,2	100,5	3,3
18	39,1	382,4	4,7
19	47,7	405,2	5,4
20	70,2	1225,9	7,8

Table 18: *Results of area phase fraction studies of material 4 heat treated at 1120° C*

Location	Ferrite bandwidth [μm]	Inspected Area [μm^2]	Area fraction [%]
1	45,9	493,5	3,3
2	26	138,3	1,2
3	35,7	288,9	2,3
4	48,2	311,2	3,1
5	77,7	1435,3	3,9
6	37,9	257,5	2,5
7	27,1	128	1,3
8	30,5	209,2	1,5
9	51,8	377,1	3,5
10	65,4	811,6	3,4
11	30,8	206,2	1,7
12	24,2	107,8	1,8
13	61,4	789	3,5
14	33,3	204,6	3,1
15	28	204,6	2,5
16	48,9	378,3	3,1
17	35,6	173,8	2,8
18	41,3	323	3
19	36	482	2,4
20	64,8	416,9	3,4

Table 19: *Results of area phase fraction studies of material 4 heat treated at 1160° C*

Location	Ferrite bandwidth [μm]	Inspected Area [μm^2]	Area fraction [%]
1	36	298,7	3,3
2	24,3	146,2	2,4
3	37	300,4	3,1
4	31,2	204,7	3,3
5	48	522,5	4,1
6	31,4	226,5	3
7	40,6	396,9	4
8	30	164	2,4
9	46,3	439,1	4,2
10	28,7	141,2	2,7
11	43,7	414,3	3,8
12	22,4	116,2	2
13	34,3	222,6	3,3
14	82,9	814,8	5,4
15	53,1	766,8	4,7
16	59,9	526,4	5,1
17	33,1	160,6	3,2
18	39,7	416,9	3,7
19	73,2	1442,7	5,2
20	20,4	151,4	1,2

Appendix B – Results from microhardness tests

The results from the microhardness tests for all the samples at the various heat treatment temperatures are listed in the tables below:

Table 20: *Results of microhardness test of material 1 in the as received condition*

Indentation nr.	$HV_{0.2}$ Ferrite	Ferrite bandwidth [μm]	$HV_{0.2}$ Austenite
1	287	78,2	267
2	277	50,9	280
3	292	71,9	278
4	295	82,5	269
5	285	80,4	252
6	307	87,7	268
7	298	76,3	279
8	288	90,6	269
9	306	78,6	254
10	298	54,6	261
11	290	74,6	272
12	321	78,1	274
13	306	62,3	262
14	300	60,8	278
15	294	118,8	281

Table 21: *Results of microhardness test of material 1 heat treated at 1060°C*

Indentation nr.	$HV_{0.2}$ Ferrite	Ferrite bandwidth [μm]	$HV_{0.2}$ Austenite
1	316	71,3	272
2	309	58,8	268
3	321	74,5	272
4	305	85,2	278
5	304	73,5	284
6	316	74,1	264
7	312	57,8	297
8	342	53	261
9	298	66,7	281
10	315	51,4	273
11	324	68	266
12	295	66,2	275
13	294	60,3	296
14	284	63,1	281
15	296	61,5	281

Table 22: *Results of microhardness test of material 1 heat treated at 1120°C*

Indentation nr.	$HV_{0.2}$ Ferrite	Ferrite bandwidth [μm]	$HV_{0.2}$ Austenite
1	362	87,3	291
2	364	60,4	289
3	329	49,7	284
4	331	61,8	302
5	338	56,3	258
6	360	75,3	296
7	342	89	277
8	315	65	265
9	356	94,1	289
10	350	77,4	290
11	366	84,1	296
12	337	70,2	285
13	369	65,5	295
14	350	70,4	284
15	321	124,7	260

Table 23: *Results of microhardness test of material 1 heat treated at 1160°C*

Indentation nr.	$HV_{0.2}$ Ferrite	Ferrite bandwidth [μm]	$HV_{0.2}$ Austenite
1	338	80,6	264
2	332	78,8	276
3	345	91,2	284
4	346	74,6	254
5	346	81,7	270
6	345	83,7	278
7	340	53,3	279
8	367	93,5	299
9	360	83,6	281
10	321	59,4	274
11	371	85,9	296
12	361	93,6	271
13	364	80,2	276
14	340	49,4	283
15	363	79,4	292

Table 24: *Results of microhardness test of material 2 in the as received condition*

Indentation nr.	$HV_{0.2}$ Ferrite	Ferrite bandwidth [μm]	$HV_{0.2}$ Austenite
1	326	75,1	256
2	313	57,8	255
3	311	75,4	249
4	291	56,3	268
5	308	51,4	270
6	323	85,5	264
7	312	128	281
8	286	71,8	279
9	320	84,3	287
10	292	71,4	288
11	330	57,5	268
12	327	104,6	259
13	326	56,8	262
14	306	47	261
15	316	54	254

Table 25: *Results of microhardness test of material 2 heat treated at 1060° C*

Indentation nr.	$HV_{0.2}$ Ferrite	Ferrite bandwidth [μm]	$HV_{0.2}$ Austenite
1	330	52,2	260
2	342	56,1	271
3	307	88,5	278
4	348	105	271
5	291	53	261
6	288	77,2	255
7	338	67,3	267
8	332	60,2	256
9	295	38,9	291
10	300	60,1	259
11	297	50,9	274
12	325	47,5	279
13	315	99,5	257
14	332	57,4	266
15	323	49	280

Table 26: *Results of microhardness test of material 2 heat treated at 1120°C*

Indentation nr.	$HV_{0.2}$ Ferrite	Ferrite bandwidth [μm]	$HV_{0.2}$ Austenite
1	359	79,8	264
2	310	48,2	250
3	313	70,7	242
4	331	65,7	294
5	343	72,8	258
6	328	60,8	296
7	358	73,4	270
8	363	108,2	263
9	362	61	271
10	353	90,3	264
11	374	88,7	261
12	367	57,9	264
13	361	71	283
14	358	63,6	284
15	330	48,9	276

Table 27: *Results of microhardness test of material 2 heat treated at 1160°C*

Indentation nr.	$HV_{0.2}$ Ferrite	Ferrite bandwidth [μm]	$HV_{0.2}$ Austenite
1	320	53,4	302
2	350	61,3	266
3	354	85,2	281
4	355	63	277
5	331	58,8	263
6	354	66,5	284
7	364	110,2	260
8	371	100,2	285
9	325	109,9	263
10	373	103,4	293
11	363	61,5	258
12	381	118,7	257
13	388	91,6	248
14	378	63,7	287
15	333	78,4	283

Table 28: *Results of microhardness test of material 3 in the as received condition*

Indentation nr.	$HV_{0.2}$ Ferrite	Ferrite bandwidth [μm]	$HV_{0.2}$ Austenite
1	320	75,1	268
2	315	119,4	277
3	325	58,5	265
4	318	61,6	268
5	323	73,5	261
6	307	44,4	261
7	319	52,8	288
8	327	106,6	259
9	309	84,1	257
10	314	59,9	262
11	315	53,2	254
12	313	80,2	277
13	307	64,5	262
14	311	50,5	260
15	311	67,3	264

Table 29: *Results of microhardness test of material 3 heat treated at 1060°C*

Indentation nr.	$HV_{0.2}$ Ferrite	Ferrite bandwidth [μm]	$HV_{0.2}$ Austenite
1	290	64,5	267
2	330	68,4	258
3	289	62,3	292
4	305	69,4	267
5	269	72,4	252
6	323	64	263
7	273	115,8	245
8	357	66,6	255
9	315	79,8	259
10	345	62,3	264
11	319	54,5	280
12	318	70,7	249
13	327	69,5	269
14	350	108,4	285
15	347	60,9	264

Table 30: *Results of microhardness test of material 3 heat treated at 1120°C*

Indentation nr.	$HV_{0.2}$ Ferrite	Ferrite bandwidth [μm]	$HV_{0.2}$ Austenite
1	357	109,5	279
2	367	65,5	287
3	359	69,4	269
4	365	76,7	274
5	347	64,6	277
6	345	57,6	291
7	348	116,8	262
8	365	77	301
9	354	65,4	271
10	354	83,9	288
11	367	94,1	253
12	349	66,9	277
13	376	95,7	283
14	386	87,4	271
15	358	65	294

Table 31: *Results of microhardness test of material 3 heat treated at 1160°C*

Indentation nr.	$HV_{0.2}$ Ferrite	Ferrite bandwidth [μm]	$HV_{0.2}$ Austenite
1	357	46,8	289
2	371	81,5	275
3	384	68,7	254
4	401	87,3	250
5	343	52,3	275
6	379	72,1	296
7	322	65,2	264
8	398	80	270
9	382	67,2	283
10	342	49,8	251
11	325	45,3	246
12	381	70,1	263
13	378	74,9	263
14	373	84	260
15	386	115,9	275

Table 32: *Results of microhardness test of material 4 in the as received condition*

Indentation nr.	$HV_{0.2}$ Ferrite	Ferrite bandwidth [μm]	$HV_{0.2}$ Austenite
1	255	56,3	259
2	251	66,6	253
3	245	70,2	235
4	245	53,8	235
5	257	66,3	261
6	234	60,3	237
7	252	87,3	238
8	244	63,9	233
9	254	69,6	257
10	259	68,3	249
11	259	72	242
12	256	59,9	234
13	247	57,6	254
14	257	60,5	236
15	266	60	257

Table 33: *Results of microhardness test of material 4 heat treated at 1060°C*

Indentation nr.	$HV_{0.2}$ Ferrite	Ferrite bandwidth [μm]	$HV_{0.2}$ Austenite
1	260	93,5	249
2	289	76,5	262
3	273	53,5	273
4	256	65,2	273
5	277	52,3	253
6	262	107,1	257
7	255	56,3	262
8	287	74,6	245
9	295	62,5	256
10	284	53,7	260
11	295	62,2	259
12	277	49,2	253
13	300	82,1	273
14	296	43,9	266
15	268	63,6	247

Table 34: *Results of microhardness test of material 4 heat treated at 1120°C*

Indentation nr.	$HV_{0.2}$ Ferrite	Ferrite bandwidth [μm]	$HV_{0.2}$ Austenite
1	321	52,4	263
2	325	71,1	264
3	326	64,6	280
4	287	51,2	275
5	324	74,5	259
6	304	99,8	244
7	325	73,2	255
8	298	43,1	280
9	319	54,6	241
10	307	57,4	281
11	291	49,5	265
12	288	60,3	273
13	317	52,1	284
14	273	59,2	281
15	311	83	281

Table 35: *Results of microhardness test of material 4 heat treated at 1160°C*

Indentation nr.	$HV_{0.2}$ Ferrite	Ferrite bandwidth [μm]	$HV_{0.2}$ Austenite
1	312	72,4	279
2	287	64,9	250
3	274	54,2	255
4	307	60,7	264
5	304	70,3	267
6	295	87,2	255
7	290	46,7	254
8	293	65,6	229
9	309	77,3	266
10	287	59,8	253
11	319	75,6	281
12	322	89,6	245
13	296	71,6	260
14	289	75,4	252
15	309	106,9	276

Table 36: *Results of microhardness test of material A in the as received condition*

Indentation nr.	$HV_{0.2}$ Ferrite	Ferrite bandwidth [μm]	$HV_{0.2}$ Austenite
1	281	96,8	268
2	272	74,1	268
3	287	62,4	261
4	268	58,6	245
5	290	93,5	255
6	295	65,3	261
7	265	58,8	271
8	309	92,1	271
9	275	65,2	272
10	301	86,1	298
11	278	76,5	250
12	273	83,3	253
13	282	105	266
14	276	106,6	254
15	270	62,6	282

Table 37: *Results of microhardness test of material A heat treated at 1060° C*

Indentation nr.	$HV_{0.2}$ Ferrite	Ferrite bandwidth [μm]	$HV_{0.2}$ Austenite
1	297	62,3	272
2	283	49,8	279
3	280	60,5	250
4	319	72,4	273
5	320	59,3	290
6	283	68,9	264
7	283	57,6	283
8	316	49,8	253
9	285	111,7	275
10	308	81,6	270
11	312	57,7	275
12	293	66,1	275
13	302	68,9	292
14	305	47	259
15	307	42,7	266

Table 38: *Results of microhardness test of material A heat treated at 1120° C*

Indentation nr.	$HV_{0.2}$ Ferrite	Ferrite bandwidth [μm]	$HV_{0.2}$ Austenite
1	335	66,2	265
2	321	74,8	278
3	313	95,1	275
4	321	61,6	297
5	294	70,4	262
6	326	72,4	303
7	302	97,2	282
8	312	83,4	312
9	323	111,2	307
10	319	70,7	286
11	314	123,3	272
12	325	81,4	307
13	290	58,8	277
14	327	71,7	258
15	332	112,9	269

Table 39: *Results of microhardness test of material A heat treated at 1160° C*

Indentation nr.	$HV_{0.2}$ Ferrite	Ferrite bandwidth [μm]	$HV_{0.2}$ Austenite
1	313	83,1	280
2	308	64,3	303
3	329	106,9	260
4	340	118,6	270
5	339	86,7	280
6	342	85,5	270
7	310	73,8	264
8	321	99,7	281
9	330	55	264
10	334	65,3	300
11	330	70,9	278
12	328	71	281
13	326	102	277
14	322	48	267
15	324	68,8	272

Table 40: *Results of microhardness test of material B in the as received condition*

Indentation nr.	$HV_{0.2}$ Ferrite	Ferrite bandwidth [μm]	$HV_{0.2}$ Austenite
1	296	56,7	268
2	301	70,1	270
3	281	66	292
4	303	63,8	266
5	285	63	286
6	299	74,2	283
7	294	77,6	280
8	310	72,4	300
9	285	80,7	283
10	304	54,1	292
11	313	74,2	291
12	313	121,7	296
13	307	62	262
14	295	56,8	248
15	288	92,3	285

Table 41: *Results of microhardness test of material B heat treated at 1060° C*

Indentation nr.	$HV_{0.2}$ Ferrite	Ferrite bandwidth [μm]	$HV_{0.2}$ Austenite
1	294	68	252
2	289	53	256
3	294	52,8	279
4	289	85,6	256
5	303	69,1	268
6	299	54,1	288
7	280	61,4	262
8	300	59,4	272
9	302	101,5	295
10	292	63,6	273
11	284	56,7	272
12	316	89	287
13	276	72	269
14	298	80,5	298
15	296	83,2	267

Table 42: *Results of microhardness test of material B heat treated at 1120° C*

Indentation nr.	$HV_{0.2}$ Ferrite	Ferrite bandwidth [μm]	$HV_{0.2}$ Austenite
1	324	65,2	271
2	355	80,5	288
3	340	98,2	299
4	293	53,4	251
5	324	90,3	267
6	323	71,6	290
7	344	80,1	258
8	350	96,4	281
9	326	61,8	299
10	301	51,7	258
11	342	106,9	277
12	328	50,6	300
13	333	61	276
14	322	75,4	257
15	316	58	300

Table 43: *Results of microhardness test of material B heat treated at 1160° C*

Indentation nr.	$HV_{0.2}$ Ferrite	Ferrite bandwidth [μm]	$HV_{0.2}$ Austenite
1	314	58,5	262
2	311	63,6	259
3	323	79	281
4	343	85,4	262
5	329	79,7	265
6	313	49,6	291
7	338	117,8	258
8	316	70,8	256
9	332	105	264
10	330	65,6	280
11	325	53,7	305
12	325	66,7	277
13	336	78,3	273
14	320	66	310
15	336	79,8	291

Table 44: *Results of microhardness test of material C in the as received condition*

Indentation nr.	$HV_{0.2}$ Ferrite	Ferrite bandwidth [μm]	$HV_{0.2}$ Austenite
1	294	61,2	257
2	289	73	257
3	304	74,4	276
4	287	79	271
5	314	87,4	269
6	301	57,9	284
7	282	77,4	274
8	305	72,2	267
9	320	70,8	268
10	301	58,2	288
11	327	63,5	285
12	297	56,7	248
13	304	78,9	290
14	306	75,6	290
15	290	77,4	294

Table 45: *Results of microhardness test of material C heat treated at 1060° C*

Indentation nr.	$HV_{0.2}$ Ferrite	Ferrite bandwidth [μm]	$HV_{0.2}$ Austenite
1	289	61,2	257
2	280	73	257
3	295	74,4	276
4	334	79	271
5	270	87,4	269
6	317	57,9	284
7	288	77,4	274
8	317	72,2	267
9	326	70,8	268
10	290	58,2	288
11	317	63,5	285
12	308	56,7	248
13	321	78,9	290
14	301	75,6	290
15	303	77,4	294

Table 46: *Results of microhardness test of material C heat treated at 1120° C*

Indentation nr.	$HV_{0.2}$ Ferrite	Ferrite bandwidth [μm]	$HV_{0.2}$ Austenite
1	339	80	264
2	303	54	289
3	290	68,6	276
4	313	68,7	300
5	319	59,8	274
6	315	95,3	289
7	368	92,2	292
8	314	86	292
9	331	57,3	285
10	337	88,6	268
11	348	81,8	295
12	305	60,7	259
13	306	63,6	271
14	307	67,7	263
15	329	69,3	275

Table 47: *Results of microhardness test of material C heat treated at 1160° C*

Indentation nr.	$HV_{0.2}$ Ferrite	Ferrite bandwidth [μm]	$HV_{0.2}$ Austenite
1	333	91	254
2	337	55,6	268
3	298	85	283
4	354	60,6	279
5	372	73,4	263
6	377	59,8	264
7	323	103,1	243
8	350	141,8	260
9	310	78,2	274
10	353	94,2	290
11	336	75,9	264
12	319	104,2	263
13	349	63	273
14	350	66,3	286
15	328	57	245

Table 48: *Results of microhardness test of material D in the as received condition*

Indentation nr.	$HV_{0.2}$ Ferrite	Ferrite bandwidth [μm]	$HV_{0.2}$ Austenite
1	296	87,4	270
2	285	85,8	265
3	267	53,2	283
4	303	83,3	235
5	293	69,7	269
6	320	96,1	275
7	301	70,5	276
8	287	83	271
9	277	100	268
10	298	86	257
11	285	82,8	246
12	291	70,4	262
13	272	99,7	251
14	311	100,8	268
15	306	88,9	270

Table 49: *Results of microhardness test of material D heat treated at 1060° C*

Indentation nr.	$HV_{0.2}$ Ferrite	Ferrite bandwidth [μm]	$HV_{0.2}$ Austenite
1	302	107,2	269
2	301	93	251
3	296	71,5	253
4	324	65	265
5	274	57,5	252
6	311	48,2	258
7	339	70,1	274
8	272	105,7	265
9	307	57,5	269
10	318	67	237
11	316	94,2	244
12	317	59,9	272
13	296	68,4	280
14	311	77,7	292
15	321	84,4	274

Table 50: *Results of microhardness test of material D heat treated at 1120° C*

Indentation nr.	$HV_{0.2}$ Ferrite	Ferrite bandwidth [μm]	$HV_{0.2}$ Austenite
1	340	159,1	257
2	360	110,8	278
3	370	79,8	285
4	381	82,7	319
5	348	94,4	315
6	341	91,1	275
7	316	44	266
8	363	68,7	276
9	371	71,5	270
10	341	165,5	266
11	342	84,5	287
12	377	76,9	257
13	350	100,7	256
14	317	71,7	300
15	387	104	286

Table 51: *Results of microhardness test of material D heat treated at 1160° C*

Indentation nr.	$HV_{0.2}$ Ferrite	Ferrite bandwidth [μm]	$HV_{0.2}$ Austenite
1	386	78,3	277
2	386	113,7	258
3	357	63,1	284
4	354	48,2	261
5	383	99	285
6	323	71,7	304
7	382	102,8	294
8	391	69,1	289
9	385	93,7	286
10	316	85,4	295
11	362	61,7	270
12	336	84,7	300
13	370	71,9	251
14	378	77,7	273
15	356	85,9	259

Table 52: *Results of microhardness test of material E in the as received condition*

Indentation nr.	$HV_{0.2}$ Ferrite	Ferrite bandwidth [μm]	$HV_{0.2}$ Austenite
1	361	66,4	309
2	353	69,4	296
3	340	88,5	294
4	331	85,9	267
5	351	106,6	303
6	358	66,4	265
7	347	57,2	314
8	347	63,4	263
9	333	56,1	309
10	312	70,1	267
11	354	76,1	269
12	361	65,7	298
13	359	71,9	270
14	363	64,8	313
15	350	72	299

Table 53: *Results of microhardness test of material E heat treated at 1060° C*

Indentation nr.	$HV_{0.2}$ Ferrite	Ferrite bandwidth [μm]	$HV_{0.2}$ Austenite
1	327	87,8	291
2	320	56,9	304
3	341	78,6	296
4	372	104,2	294
5	318	53,1	329
6	330	67,9	300
7	352	44,1	314
8	370	126,2	256
9	340	55,6	323
10	336	94,4	313
11	350	54,3	288
12	340	72,2	292
13	345	56	329
14	353	67,8	287
15	362	62,2	313

Table 54: *Results of microhardness test of material E heat treated at 1120° C*

Indentation nr.	$HV_{0.2}$ Ferrite	Ferrite bandwidth [μm]	$HV_{0.2}$ Austenite
1	344	77,1	313
2	393	84,5	277
3	369	77,8	296
4	377	62,1	317
5	381	89,1	300
6	355	62,1	287
7	365	64,1	289
8	334	57,5	309
9	389	80,6	273
10	353	91,9	310
11	367	93,7	339
12	376	53,2	291
13	397	70,2	307
14	387	86,5	316
15	386	60,4	261

Table 55: *Results of microhardness test of material E heat treated at 1160° C*

Indentation nr.	$HV_{0.2}$ Ferrite	Ferrite bandwidth [μm]	$HV_{0.2}$ Austenite
1	363	67,1	302
2	415	101,4	317
3	368	45,6	327
4	413	74,4	341
5	387	69,9	330
6	373	120,4	312
7	345	56,6	265
8	418	117,7	289
9	380	59,4	305
10	394	89,3	330
11	399	70,6	357
12	410	55,2	302
13	407	55,8	314
14	346	80,4	354
15	409	86,8	321

Table 56: *Results of microhardness test of material F in the as received condition*

Indentation nr.	$HV_{0.2}$ Ferrite	Ferrite bandwidth [μm]	$HV_{0.2}$ Austenite
1	309	70,1	248
2	304	75,8	265
3	304	84,3	243
4	313	93,9	255
5	290	69,5	255
6	290	145	269
7	292	76,7	268
8	297	131	275
9	312	107,8	263
10	285	83,2	259
11	302	84,9	289
12	297	70,5	288
13	288	47,5	265
14	318	154,3	285
15	281	72,8	269

Table 57: *Results of microhardness test of material F heat treated at 1060° C*

Indentation nr.	$HV_{0.2}$ Ferrite	Ferrite bandwidth [μm]	$HV_{0.2}$ Austenite
1	337	112,6	265
2	278	87,7	250
3	352	93,2	298
4	319	80,7	240
5	329	118,9	243
6	294	65,6	249
7	327	73,7	256
8	342	104,8	263
9	338	90	270
10	303	90,4	269
11	323	56,6	241
12	323	80,6	242
13	351	146,4	251
14	345	95,3	236
15	349	82,8	254

Table 58: *Results of microhardness test of material F heat treated at 1120° C*

Indentation nr.	$HV_{0.2}$ Ferrite	Ferrite bandwidth [μm]	$HV_{0.2}$ Austenite
1	352	131	267
2	366	79,9	248
3	364	119,5	255
4	343	152	256
5	317	70,1	297
6	352	75,9	248
7	356	123,1	246
8	355	84,9	273
9	384	91,9	246
10	366	150,2	260
11	372	86,5	305
12	341	93,1	263
13	365	95	266
14	362	135,3	260
15	320	85,3	258

Table 59: *Results of microhardness test of material F heat treated at 1160° C*

Indentation nr.	$HV_{0.2}$ Ferrite	Ferrite bandwidth [μm]	$HV_{0.2}$ Austenite
1	341	62,2	278
2	371	132,8	261
3	362	97,1	260
4	323	116,3	256
5	363	92	266
6	342	65	268
7	378	85,3	258
8	354	156,6	262
9	381	101,8	301
10	354	71,2	253
11	379	99,9	241
12	356	130,4	245
13	362	70,2	252
14	341	131	238
15	348	103,3	251